Top-induced contributions to $H \to b\bar{b}$ and $H \to c\bar{c}$ at $\mathcal{O}(\alpha_s^3)$

Roberto Mondini, Ulrich Schubert and Ciaran Williams

Department of Physics, University at Buffalo, The State University of New York,
239 Fronczak Hall, Buffalo, NY 14260, U.S.A.

E-mail: rmondini@buffalo.edu, ulrichsc@buffalo.edu,
ciaranwi@buffalo.edu

ABSTRACT: In this paper we present a fully-differential calculation for the contributions to the partial widths $H \to b\bar{b}$ and $H \to c\bar{c}$ that are sensitive to the top quark Yukawa coupling y_t to order α_s^3. These contributions first enter at order α_s^2 through terms proportional to $y_t y_q$ $(q = b, c)$. At order α_s^3 corrections to the mixed terms are present as well as a new contribution proportional to y_t^2. Our results retain the mass of the final-state quarks throughout, while the top quark is integrated out resulting in an effective field theory (EFT). Our results are implemented into a Monte Carlo code allowing for the application of arbitrary final-state selection cuts. As an example we present differential distributions for observables in the Higgs boson rest frame using the Durham jet clustering algorithm. We find that the total impact of the top-induced (i.e. EFT) pieces is sensitive to the nature of the final-state cuts, particularly b-tagging and c-tagging requirements. For bottom quarks, the EFT pieces contribute to the total width (and differential distributions) at around the percent level. The impact is much bigger for the $H \to c\bar{c}$ channel, with effects as large as 15%. We show however that their impact can be significantly reduced by the application of jet-tagging selection cuts.

KEYWORDS: Higgs Physics, Perturbative QCD

ARXIV EPRINT: 2006.03563

Contents

1 Introduction

The seminal moment in particle physics of the last twenty years was the discovery of the Higgs boson in 2012 by the ATLAS and CMS experiments at CERN's Large Hadron Collider (LHC) [1, 2]. In the years since its discovery the continued study of the Higgs boson has become one of the key missions of high energy physics. The global properties of the Higgs boson (its spin, mass, and parity) are by now well constrained [3]. Going forward, of particular interest is the study of the Higgs boson couplings to other particles in the Standard Model (SM) and itself. The Higgs boson self-coupling, fully predicted in the SM from known parameters, awaits experimental verification (or contradiction) and represents a key to understanding the large-scale picture of Electroweak (EW) symmetry breaking.

Over the course of Run I and Run II of the LHC, constraints on the couplings of the Higgs boson to particles in the SM have significantly improved [3–6] and should continue to do so over the forthcoming Run III and subsequent HL-LHC runs over the next couple of decades [7]. Complimentary to the continued study at a hadron machine, plans are afoot

to construct a next-generation lepton collider [8–10]. Such a machine would offer a pristine environment in which to study the Higgs boson, with sub-percentage measurements of couplings across the board.

Constraints on, and measurements of, the couplings of the Higgs boson proceed through measurements of its different production and decay mechanisms. Of the decay channels, $H \to b\bar{b}$ is particularly important. For the 125 GeV Higgs boson, $H \to b\bar{b}$ has a large branching fraction ($\sim 50\%$) and therefore dominates the total decay width of the Higgs boson. Uncertainties in the measurement of the Higgs-bottom coupling propagate through to every measurement of the (on-shell) Higgs boson through its dependence on the total width. Extended Higgs sectors (which naturally arise in Beyond the Standard Model (BSM) scenarios) can alter the relative coupling of up-type and down-type quarks to the Higgs boson, so that constraining the $H \to b\bar{b}$ process can in turn lead to constrains on extended Higgs sectors. For these reasons, it is thus highly desirable to study $H \to b\bar{b}$ as accurately as possible. In addition, another long-term goal of the Higgs program is to directly measure the decay of the Higgs boson to the second-generation particles (specifically, muons and charms). Such a measurement would concretely establish the validity of the Higgs mechanism in the SM more broadly than existing third-generation and vector boson studies. A measurement of $H \to c\bar{c}$ experimentally is extremely challenging, given the rampant QCD backgrounds, difficulties in charm-tagging, and smaller branching fraction. Nevertheless exciting progress has been made recently, with analyses reporting first direct constraints on $\sigma \times \mathcal{BR}$ in associated production at the LHC [11, 12].

Beyond the obvious challenges associated with making a sub-percentage precision measurement at the LHC or a Future Collider (FC), there are several theoretical issues which must be addressed. First and foremost, the parameter which is being extracted from the theory needs to carefully considered. At leading order in perturbation theory the identification $y_b = m_b/v$ is made, where y_b is the bottom Yukawa coupling we seek to constrain, m_b is the bottom-quark mass, and v is the vacuum expectation value. At LO the partial width $\Gamma_{H \to b\bar{b}}$ is proportional to y_b^2, and thus y_b could be readily extracted from the decay rate of $H \to b\bar{b}$ (as part of a global fit).

The quantities in $y_b = m_b/v$ are defined at leading order in terms of bare Lagrangian parameters, and require appropriate renormalization at higher orders in perturbation theory. Although the bottom quark is not an isolated stable particle, for perturbative predictions of $\Gamma_{H \to b\bar{b}}$ it is treated as such, and accordingly it is convenient to use the on-shell renormalization scheme to define the mass at higher orders. Preserving the relationship $y_b = m_b/v$ would therefore also suggest evaluating the Yukawa coupling in the on-shell scheme. However, it was noted long ago in the first computations of $H \to b\bar{b}$ at next-to-leading order [13] that employing the on-shell scheme results in large higher-order effects. These effects can be compensated if, instead of evaluating y_b in the on-shell scheme, one chooses the $\overline{\text{MS}}$ scheme. A feature of the $\overline{\text{MS}}$ scheme is that it allows one to evolve the couplings to different scales, where for instance the bottom-quark mass entering the definition of the Yukawa coupling is evaluated not near the bottom pole mass, but at the Higgs boson mass. By capturing the relevant logarithms in the running the subsequent higher order predictions using $y_b^{\overline{\text{MS}}}$ are more convergent. This then defines a mixed renormalization scheme,

in which there are effectively two bottom quark masses: the $\overline{\text{MS}}$ mass that enters the definition of the Yukawa coupling and the kinematic mass that enters the rest of the calculation (e.g. the propagators, completeness relations etc). When comparing to experimental data we therefore constrain $y_b^{\overline{\text{MS}}}$. A further advantage of this scheme is that, by treating the kinematic bottom quark mass as different from the coupling mass, one can take a simplified limit where the former goes to zero (henceforth referred to as the "massless" approximation).

Further complications arise at higher order (beyond the parameter definition just discussed) since we need to consider Feynman diagrams in which the bottom quark does not directly couple to the Higgs boson, but instead the Higgs couples to either top quarks or a massive vector boson, which then subsequently produce final state bottom quarks. Of particular interest in this paper is the expansion in QCD and the role of the top quark. At Next-to-Next-to Leading Order (NNLO) in QCD a term of the form $y_b y_t$ appears and Next-to-Next-to-Next-to Leading Order (N³LO) a term proportional to y_t^2 enters the prediction. Given the large hierarchy between y_t and y_b it is crucial to understand how large the new pieces are, and in particular how they manifest themselves in collider analyses. This requires precise knowledge of both inclusive, and differential predictions of $H \to b\bar{b}$ at a suitably high order in perturbation theory. We note that in the massless limit the contribution from the $y_t y_b$ pieces vanishes, due to the presence of a helicity flip. These pieces are likely to be even more important in the decay $H \to c\bar{c}$ due to the large hierarchy $y_t \gg y_c$, and potential quasi-collinear enhancements.

Much work has gone into computing inclusive rates for $H \to b\bar{b}$ over several decades [13–21] and as such, higher-order corrections from QCD for the inclusive decay width are known up to N⁴LO (i.e. up to order $\mathcal{O}(\alpha_s^4)$) [22]. Additionally, the electroweak (EW) corrections have been known for some time [23], as well as the mixed QCD×EW corrections ($\mathcal{O}(\alpha\alpha_s)$) [24] and the two-loop master integrals for the mixed QCD×EW corrections for the Higgs-top Yukawa coupling contributions to $H \to b\bar{b}$ have also been computed [25]. There has also been significant recent progress on computing differential predictions more relevant for collider analyses. Fully-differential predictions at NNLO in QCD were computed several years ago [26, 27] in the massless limit and more recently including the full kinematic effects of the bottom quark mass [28, 29]. The massless limit was extended to a fully differential N³LO prediction recently [30, 31].[1]

In this paper we therefore aim to complete the computation at $\mathcal{O}(\alpha_s^3)$ by extending the results of ref. [30] to include the pieces proportional to y_t. In order to do so we will retain the mass of the bottom quark throughout the computation, but integrate out the top quark in order to produce an Effective Field Theory (EFT). Our paper proceeds as follows, in section 2 we outline the details of our calculation, including further discussion of the mixed renormalization scheme, and the IR structure of our calculation. Differential results for $H \to b\bar{b}$ are presented in section 3 and for $H \to c\bar{c}$ in section 4. We draw our conclusions in section 5. Two appendices contain technical parameters and specifications related to our calculation.

---

[1]A component of the N³LO calculation is the two-loop $H \to b\bar{b}g$ amplitudes, which have been calculated in ref. [32].

Figure 1. Representative Feynman diagrams for the "LO" contributions to the processes discussed in this paper, there are two separate processes corresponding to two-body, and three-body decays of the Higgs. Both processes occur through an interference of a traditional y_b amplitude, with an EFT induced amplitude.

2 Calculation

2.1 Overview

In this section we present an overview of our calculation, focusing for now on the decay $H \rightarrow b\bar{b}$. We begin by discussing the general features of the top-initiated contributions. When performing this calculation, one of the initial decisions that must be made is how to handle the top quark itself. The complexity of the calculation can be reduced considerably if the top quark is integrated out of the theory, resulting in an effective field theory (EFT) of QCD with n_l massless and n_h massive flavors. In terms of the bare parameters (denoted by a B label), the relevant parts of the subsequent Lagrangian can be written as

$$
\begin{aligned}
\mathcal{L} = {} & \mathcal{L}_g^{\mathrm{QCD}} + \frac{1}{2}((\partial_\mu H)^2 - m_H^2 H^2) - V_{SM}(H) \\
& + \sum_{j \in \{n_l\}} \overline{\psi}_j^B (i\not{D}) \psi_j^B \\
& + \sum_{j \in \{n_h\}} \left(\overline{\psi}_j^B (i\not{D} - m_j^B) \psi_j^B - y_j^B C_2^B \, H \overline{\psi}_j^B \psi_j^B \right) \\
& - \frac{C_1^B}{v} H G_{\mu\nu}^{B,a} G_{B,a}^{\mu\nu}.
\end{aligned}
\tag{2.1}
$$

In the above Lagrangian C_1 and C_2 are matching parameters which relate the EFT to the SM, diagrams illustrating their generation are shown in figure 2. The symbol $\not{D}$ defines the covariant derivative which couples the gluon field A_μ^B to the fermions ψ_j^B. The term $V_{SM}(H)$ defines the triple and quartic interactions of the Higgs boson (which are not needed for our calculation), and $\mathcal{L}_g^{\mathrm{QCD}}$ collects all of the kinetic terms for the gluons, ghost, and gauge-fixing terms required to define the QCD Lagrangian. We will discuss the relationship between the bare parameters and the renormalized ones in the next subsection. The differences arising between the full SM and the EFT have been studied for our process of interest at $\mathcal{O}(\alpha_s^2)$ in ref. [33], finding very small differences between the two prescriptions, thus motivating the application of the EFT to $\mathcal{O}(\alpha_s^3)$. For the remainder of this paper we will work in the EFT defined above, but will frequently refer to the EFT pieces as "top-induced" for ease of discussion.

At $\mathcal{O}(\alpha_s^2)$ there are two distinct processes which give rise to top-induced contributions. These can be classified according to the number of final-state partons present (either two or three). Representative Feynman diagrams for the two different processes are presented in
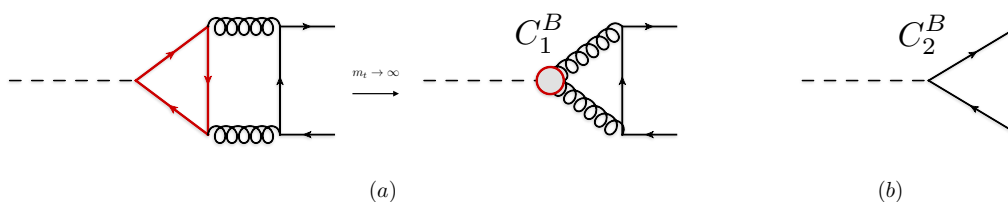
Figure 2. The generation of C_1 and C_2, (a) illustrates the generation of the Hgg operator (with subsequent coupling to bottom quarks relevant for this paper). Shown is the SM (left) in which the top quark (red) circulates in the loop, after integrating out the top quark the diagram on the right is generated with a coupling proportional to C_1. On the rightmost side (b) illustrates the C_2 coupling, which at lowest order matches the SM coupling between a Higgs boson and bottom quarks.

figure 1, which correspond to two-body and three-body decays of the Higgs boson. As can be seen from the figure, both processes occur through an interference between two types of amplitudes, an EFT amplitude in which the Higgs boson couples to gluons, and the pure-y_b amplitude in which the Higgs boson couples directly to the bottom quarks. The two phase-space contributions which occur as part of the $\mathcal{O}(\alpha_s^2)$ corrections are separately IR finite, with the two-body term requiring UV renormalization (of y_b).

The production of the $b\bar{b}$ pair in the EFT amplitude always occurs through their coupling to the spin-1 gluon, whereas in the y_b amplitude the quarks couple to the scalar Higgs. As a result, a mass term is needed to ensure a non-vanishing trace upon interference and accordingly the whole contribution will scale as

$$2\mathrm{Re}(A_{\mathrm{EFT}}^{\dagger} A_{y_b}) \sim y_b \frac{m_b}{v}. \tag{2.2}$$

This scaling can be used to make the argument that these terms are effectively proportional to y_b^2 and are thus of the same order as the remainder of the NNLO QCD contribution. Broadly defined this argument is valid, but care must be taken at the level of the full calculation, especially in regards to the mixed renormalization scheme which is common in the literature (and we will employ here). While a detailed overview of our renormalization prescription is provided in section 2.2, here we simply note that, following the discussion outlined in the introduction, we work in the mixed scheme and as such the scaling equation (2.2) would be written as

$$2\mathrm{Re}(A_{\mathrm{EFT}}^{\dagger} A_{y_b}) \sim y_b^{\overline{\mathrm{MS}}} y_b^{\mathrm{OS}}. \tag{2.3}$$

Due to the running of the bottom-quark mass $y_b^{\mathrm{OS}} \sim 2y_b^{\overline{\mathrm{MS}}}(m_H)$, and as such these contributions are somewhat enhanced compared to the $(y_b^{\overline{\mathrm{MS}}})^2$ which multiplies the rest of the NNLO coefficient.

At $\mathcal{O}(\alpha_s^3)$ there are three types of phase-space contributions, for which example diagrams are presented in figure 3. There are virtual corrections to the 2-body phase-space, and a 4-body phase-space contribution which corresponds to the real corrections to the 3-body phase-space. The 3-body phase-space itself has a rather intricate IR structure at this order. It contains both explicit IR poles arising from the one-loop integration, and
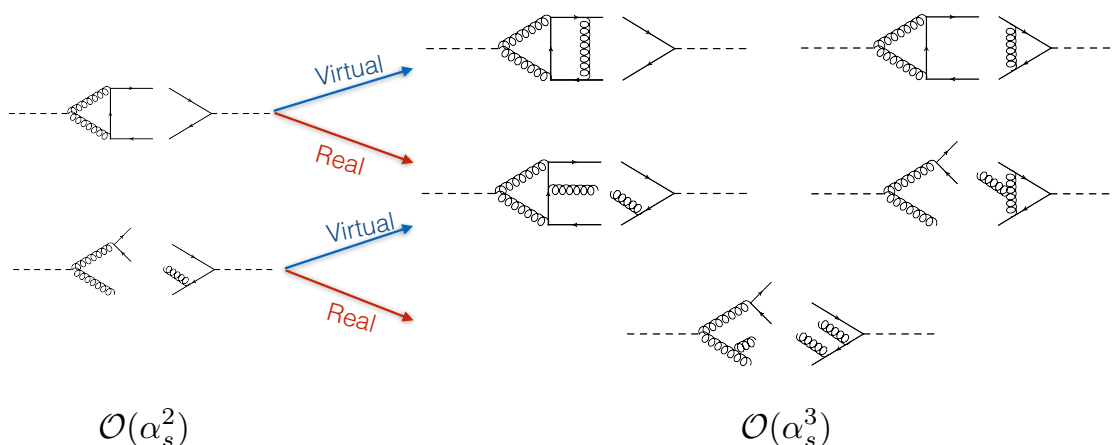
Figure 3. Representative Feynman diagrams for the EFT-induced contributions at order $\mathcal{O}(\alpha_s^3)$ computed in this paper. Unlike at $\mathcal{O}(\alpha_s^2)$ (left), the different phase-space contributions are no longer separately infrared finite. The three-body phase-space contribution is particularly complicated since it has contributions which correspond to the real corrections for the two-body final-state, with the total contribution serving as the virtual corrections to the 3-body final-state.

implicit poles which arise when the emitted gluon becomes soft. This term therefore is more akin to a real-virtual correction in a NNLO calculation.

2.2 Amplitude definitions and UV renormalization

The Higgs-to-partons amplitudes (required for our calculation) can be expanded in terms of the bare coefficients C_1^B and C_2^B (defined in eq. (2.1)) as follows,

$$\mathcal{A}_{b\bar{b}}^B \left(\alpha_s^B, m_b^B \right) = y_b^B \, C_2^B \, \mathcal{A}_{b\bar{b},C_2} \left(\alpha_s^B, m_b^B \right) + \frac{C_1^B}{v} \mathcal{A}_{b\bar{b},C_1} \left(\alpha_s^B, m_b^B \right) \tag{2.4}$$

$$\mathcal{A}_{b\bar{b}g}^B \left(\alpha_s^B, m_b^B \right) = y_b^B \, C_2^B \, \mathcal{A}_{b\bar{b}g,C_2} \left(\alpha_s^B, m_b^B \right) + \frac{C_1^B}{v} \mathcal{A}_{b\bar{b}g,C_1} \left(\alpha_s^B, m_b^B \right) \tag{2.5}$$

$$\mathcal{A}_{b\bar{b}ff}^B \left(\alpha_s^B, m_b^B \right) = y_b^B \, C_2^B \, \mathcal{A}_{b\bar{b}ff,C_2} \left(\alpha_s^B, m_b^B \right) + \frac{C_1^B}{v} \mathcal{A}_{b\bar{b}ff,C_1} \left(\alpha_s^B, m_b^B \right) , \tag{2.6}$$

where we recall that C_1^B defines the terms which couple through the EFT vertex, and C_2^B defines the bare Higgs-fermion vertex. In the four-parton decay amplitudes ff can be either gg, $q\bar{q}$ (with $m_q = 0$) or $b\bar{b}$. The $b\bar{b}b\bar{b}$ amplitude exists in a separate phase-space and is both UV- and IR-finite at $\mathcal{O}(\alpha_s^3)$.

The bare parameters defined in eq. (2.1) require renormalization in order to make our predictions UV-finite. Following the discussion in the introduction, we work in a mixed scheme (see also for instance the discussion in ref. [34]) in which the couplings are defined in the $\overline{\text{MS}}$ scheme, and the quark masses and wave functions are defined in the on-shell (OS) scheme. In this mixed scheme we define the renormalized quantities in terms of the

bare ones as follows,

$$A_\mu^B = \sqrt{Z_A^{\mathrm{OS}}}\, A_\mu \tag{2.7}$$

$$\alpha_s^B = Z_{\alpha_s}^{\overline{\mathrm{MS}}}\, \alpha_s \tag{2.8}$$

$$\psi_j^B = \sqrt{Z_Q^{\mathrm{OS}}}\, \psi_j \tag{2.9}$$

$$m_j^B = Z_m^{\mathrm{OS}}\, m_j \tag{2.10}$$

$$y_j^B = Z_{y_j}^{\overline{\mathrm{MS}}}\, y_j\,. \tag{2.11}$$

Expansion of the Z_i^S coefficients are provided to the required accuracy in appendix A. The renormalization of the Wilson coefficients is defined as follows,

$$\begin{pmatrix} C_1^B \\ C_2^B \end{pmatrix} = \begin{pmatrix} Z_{11}^{\overline{\mathrm{MS}}} & 0 \\ Z_{21}^{\overline{\mathrm{MS}}} & 1 \end{pmatrix} \begin{pmatrix} C_1 \\ C_2 \end{pmatrix} \tag{2.12}$$

with

$$Z_{11}^{\overline{\mathrm{MS}}} = 1 + \alpha_s \frac{\partial \log(Z_{\alpha_s}^{\overline{\mathrm{MS}}})}{\partial \alpha_s} \tag{2.13}$$

$$Z_{21}^{\overline{\mathrm{MS}}} = -\alpha_s \frac{\partial \log(Z_m^{\overline{\mathrm{MS}}})}{\partial \alpha_s}\,. \tag{2.14}$$

After renormalization we can define the two-parton and three-parton decay amplitudes as follows (the four-parton amplitude does not require UV renormalization at $\mathcal{O}(\alpha_s^3)$),

$$\mathcal{A}_{b\bar{b}}(\alpha_s, m_b) = Z_Q^{\mathrm{OS}} \Big[y_b\, C_2\, Z_{y_b}^{\overline{\mathrm{MS}}}\, \mathcal{A}_{b\bar{b},C_2}(\alpha_s, m_b) \tag{2.15}$$

$$+ \frac{C_1}{v} \left(Z_{11}^{\overline{\mathrm{MS}}}\, \mathcal{A}_{b\bar{b},C_1}(\alpha_s, m_b) + Z_m^{\overline{\mathrm{MS}}}\, Z_{21}^{\overline{\mathrm{MS}}}\, m_b^{\overline{\mathrm{MS}}}\, \mathcal{A}_{b\bar{b},C_2}(\alpha_s, m_b) \right) \Big]$$

$$\mathcal{A}_{b\bar{b}g}(\alpha_s, m_b) = Z_Q^{\mathrm{OS}} \sqrt{Z_A^{\mathrm{OS}}} \Big[y_b\, C_2\, Z_{y_b}^{\overline{\mathrm{MS}}}\, \mathcal{A}_{b\bar{b}g,C_2}(\alpha_s, m_b) \tag{2.16}$$

$$+ \frac{C_1}{v} \left(Z_{11}^{\overline{\mathrm{MS}}}\, \mathcal{A}_{b\bar{b}g,C_1}(\alpha_s, m_b) + Z_m^{\overline{\mathrm{MS}}}\, Z_{21}^{\overline{\mathrm{MS}}}\, m_b^{\overline{\mathrm{MS}}}\, \mathcal{A}_{b\bar{b}g,C_2}(\alpha_s, m_b) \right) \Big].$$

An unfortunate side effect of our scheme defined thus far is an inconsistency in the terms proportional to C_1. The two terms are separately UV divergent and are finite only when summed. The UV poles in $\mathcal{A}_{b\bar{b},C_1}$ and $\mathcal{A}_{b\bar{b}g,C_1}$, however, are proportional to the on-shell mass, whereas those from $\mathcal{A}_{b\bar{b},C_2}$ and $\mathcal{A}_{b\bar{b}g,C_2}$ have an $\overline{\mathrm{MS}}$ mass term arising from eq. (2.14). While at $\mathcal{O}(\alpha_s^2)$ (which corresponds to the known literature results) this inconsistency is of limited concern, since one can switch between the pole mass and $\overline{\mathrm{MS}}$ mass at will, care must be taken when expanding the amplitude to $\mathcal{O}(\alpha_s^3)$. In order to consistently cancel UV poles we employ the following relationship (see for example the discussion in ref. [35])

$$Z_m^{\overline{\mathrm{MS}}}\, m_b^{\overline{\mathrm{MS}}} = Z_m^{\mathrm{OS}}\, m_b \tag{2.17}$$

to re-write the affected terms, which results in the following renormalized amplitude,

$$\mathcal{A}_{b\bar{b}}\left(\alpha_s, m_b\right) = Z_Q^{\text{OS}}\bigg[y_b\, C_2\, Z_{y_b}^{\overline{\text{MS}}}\, \mathcal{A}_{b\bar{b},C_2}\left(\alpha_s, m_b\right) \tag{2.18}$$

$$+ \frac{C_1}{v}\left(Z_{11}^{\overline{\text{MS}}} \mathcal{A}_{b\bar{b},C_1}\left(\alpha_s, m_b\right) + Z_m^{\text{OS}}\, Z_{21}^{\overline{\text{MS}}}\, m_b\, \mathcal{A}_{b\bar{b},C_2}\left(\alpha_s, m_b\right)\right) \bigg]$$

$$\mathcal{A}_{b\bar{b}g}\left(\alpha_s, m_b\right) = Z_Q^{\text{OS}}\, \sqrt{Z_A^{\text{OS}}}\bigg[y_b\, C_2\, Z_{y_b}^{\overline{\text{MS}}}\, \mathcal{A}_{b\bar{b}g,C_2}\left(\alpha_s, m_b\right) \tag{2.19}$$

$$+ \frac{C_1}{v}\left(Z_{11}^{\overline{\text{MS}}} \mathcal{A}_{b\bar{b}g,C_1}\left(\alpha_s, m_b\right) + Z_m^{\text{OS}}\, Z_{21}^{\overline{\text{MS}}}\, m_b\, \mathcal{A}_{b\bar{b}g,C_2}\left(\alpha_s, m_b\right)\right) \bigg].$$

Finally, we note that C_1 and C_2 must be matched to the full SM [36], and therefore our calculation requires

$$C_1 = C_1^0\left(1 + \left(\frac{\alpha_s}{\pi}\right)\Delta_H^{(1)} + \mathcal{O}(\alpha_s^2)\right) \tag{2.20}$$

$$C_2 = C_2^0\left(1 + \left(\frac{\alpha_s}{\pi}\right)^2\Delta_F^{(2)} + \left(\frac{\alpha_s}{\pi}\right)^3\Delta_F^{(3)} + \mathcal{O}(\alpha_s^4)\right). \tag{2.21}$$

Here $C_1^0 = -\alpha_s/(12\pi)$ and $C_2^0 = 1$, and explicit forms for the required $\Delta_i^{(m)}$ are given in appendix A. In order to simplify formulae in the following section we introduce the following notation for the renormalized amplitudes,

$$\mathcal{A}_{b\bar{b}}(\alpha_s, m_b) = C_2\tilde{\mathcal{A}}_{b\bar{b},C_2} + C_1\tilde{\mathcal{A}}_{b\bar{b},C_1} \tag{2.22}$$

$$\mathcal{A}_{b\bar{b}g}(\alpha_s, m_b) = C_2\tilde{\mathcal{A}}_{b\bar{b}g,C_2} + C_1\tilde{\mathcal{A}}_{b\bar{b}g,C_1}, \tag{2.23}$$

such that the renormalized $\tilde{\mathcal{A}}$ amplitudes contain all terms apart from the overall scaling of the Wilson coefficient (recall that the $\tilde{A}_{X,C_1}$ amplitudes depend on both bare C_1 and C_2 amplitudes). When performing an expansion in α_s in the next section we will use the following notation to denote the perturbative expansion to $\mathcal{O}(\alpha_s^j)$:

$$\mathcal{A}_{b\bar{b}X}(\alpha_s, m_b) = \sum_j \mathcal{A}_{b\bar{b}X}^{(j)} + \mathcal{O}(\alpha_s^{(j+1)}), \tag{2.24}$$

where $b\bar{b}X$ defines the phase-space of interest, and j defines the number of loops in the (unrenormalized) amplitude. We find it most convenient to refer to terms by the scaling of the unmatched coefficients C_1^0 and C_2^0 so we finally expand

$$\mathcal{A}_{b\bar{b}X}^{(j)} = C_1^0\tilde{\mathcal{A}}_{b\bar{b}X,C_1}^{(j-1)} + C_2^0\tilde{\mathcal{A}}_{b\bar{b}X,C_2}^{(j)} \tag{2.25}$$

$$+ \sum_{m=1}^{j-1}\left(\frac{\alpha_s}{\pi}\right)^m\left(C_1^0\Delta_H^{(m)}\tilde{\mathcal{A}}_{b\bar{b}X,C_1}^{(j-m-1)}\right) + \sum_{m=1}^{j}\left(\frac{\alpha_s}{\pi}\right)^m\left(C_2^0\Delta_F^{(m)}\tilde{\mathcal{A}}_{b\bar{b}X,C_2}^{(j-m)}\right).$$

We note that the third term in the above equation (the sum over $\Delta_H^{(m)}$) is first non-zero at $\mathcal{O}(\alpha_s^3)$.

2.3 Partial widths for $H \to jj$

In this section we discuss the structure of the partial widths calculated in this paper. We will study various different final-state jet requirements (0-tagged, 1-btag, 2-btag etc.), hence we refer to the process as $H \to jj$, however we stress that at no stage do we include the pure $H \to gg$ amplitude. This is because our primary interest is related to the effects of the top quark (EFT pieces) on Higgs-bottom quark physics, so we will ultimately compute rates with one or two- b-tagged jets. Therefore the reader should treat $H \to jj$ as meaning $H \to 2$ jets, arising from a matrix element with at least one $b\bar{b}$ pair somewhere in the diagram. With this caveat in mind, we define the partial width for a Higgs boson decaying to n jets as follows,

$$\Gamma_{H \to nj} = \sum_{i=0}^{\infty} \Gamma_{H \to nj}^{(i)}. \tag{2.26}$$

At each order the partial width coefficient can be written as a sum over phase-space contributions,

$$\Gamma_{H \to nj}^{(i)} = \frac{1}{2m_H} \sum_{m=2}^{m_{\max}} \int |\tilde{\mathcal{A}}_m^{(i)}|^2 F_m^n(\Phi_m) d\Phi_m \tag{2.27}$$

In the above equation m represents the dimension of the phase-space which starts at 2 and increases to $m_{\max} = m + i$, $|\tilde{\mathcal{A}}_m^{(i)}|^2$ denotes an amplitude squared (at order α_s^i) for the Higgs decaying to m partons as discussed in the previous section. $F_m^n(\Phi_m)$ defines the measurement function which takes m partons (corresponding to a phase-space point Φ_m) into n jets (and applies additional requirements such as b-tagging) of course $F_m^n = 0$ if $m < n$. Here we are primarily interested in the case where the number of jets is equal to two. At LO and NLO only terms proportional to $C_2^0 = 1$ enter the expansion

$$\Gamma_{H \to jj}^{(0)} = \frac{(C_2^0)^2}{2m_H} \int |\tilde{\mathcal{A}}_{b\bar{b},C_2}^{(0)}|^2 F_2^2(\Phi_2) d\Phi_2 \tag{2.28}$$

and

$$\Gamma_{H \to jj}^{(1)} = \frac{(C_2^0)^2}{2m_H} \left(\int 2\text{Re}(\tilde{\mathcal{A}}_{b\bar{b},C_2}^{(0)\dagger} \tilde{\mathcal{A}}_{b\bar{b},C_2}^{(1)}) F_2^2(\Phi_2) d\Phi_2 \right.$$
$$\left. + \int |\tilde{\mathcal{A}}_{b\bar{b}g,C_2}^{(0)}|^2 F_3^2(\Phi_3) d\Phi_3 \right) \tag{2.29}$$

at $\mathcal{O}(\alpha_s^2)$ a term proportional to C_1^0 and $\Delta_F^{(1)}$ first appear, we define

$$\Gamma_{H \to jj}^{(2)} = \delta\Gamma_{H \to jj}^{C_2^2,(2)} + \delta\Gamma_{H \to jj}^{C_2 C_1,(0)} + \delta\Gamma_{H \to jj}^{\Delta_F^{(2)}(0)} \tag{2.30}$$

where

$$\delta\Gamma_{H \to jj}^{C_2^2,(2)} = \frac{(C_2^0)^2}{2m_H} \left(\int \left(2\text{Re}(\tilde{\mathcal{A}}_{b\bar{b},C_2}^{(0)\dagger} \tilde{\mathcal{A}}_{b\bar{b},C_2}^{(2)}) + |\tilde{A}_{b\bar{b},C_2}^{(1)}|^2 \right) F_2^2(\Phi_2) d\Phi_2 \right.$$
$$+ \int 2\text{Re}(\tilde{\mathcal{A}}_{b\bar{b}g,C_2}^{(0)\dagger} \tilde{\mathcal{A}}_{b\bar{b}g,C_2}^{(1)}) F_3^2(\Phi_3) d\Phi_3 + \sum_{ff=gg,q\bar{q}} \int |\tilde{\mathcal{A}}_{b\bar{b}ff,C_2}^{(0)}|^2 F_4^2(\Phi_4) d\Phi_4$$
$$\left. + \int |\tilde{\mathcal{A}}_{b\bar{b}b\bar{b},C_2}^{(0)}|^2 F_4^2(\Phi_4^m) d\Phi_4^m \right). \tag{2.31}$$

– 9 –

These pieces correspond to the double-virtual, real-virtual and real-real pieces of the NNLO coefficient. We note that we have separated the $H \to 4b$ phase-space (Φ_4^m) from the remainder of the four-body phase-space. For a recent discussion of their calculation including mass-effects we refer the reader to refs. [28, 29]. The pieces sensitive to the top quark are defined as

$$\delta\Gamma_{H \to jj}^{C_2 C_1,(0)} = \frac{(C_2^0 C_1^0)}{2m_H} \bigg(\int 2\text{Re}(\tilde{\mathcal{A}}_{b\bar{b},C_2}^{(0)\dagger} \tilde{\mathcal{A}}_{b\bar{b},C_1}^{(1)}) F_2^2(\Phi_2) d\Phi_2$$
$$+ \int 2\text{Re}(\tilde{\mathcal{A}}_{b\bar{b}g,C_2}^{(0)\dagger} \tilde{\mathcal{A}}_{b\bar{b}g,C_1}^{(0)}) F_3^2(\Phi_3) d\Phi_3 \bigg) \qquad (2.32)$$

In this paper eq. (2.32) defines our "LO". In reality there are effectively two LO contributions, since the two-body and three-body final states have different IR factorization properties. The final contribution at α_s^2 is simply a rescaling of the α_s^0 term arising from matching the EFT to the SM:

$$\delta\Gamma_{H \to jj}^{\Delta_F^{(2)},(0)} = \left(\frac{\alpha_s}{\pi}\right)^2 \Delta_F^{(2)} \Gamma_{H \to jj}^{(0)} \qquad (2.33)$$

We now turn our attention to the primary focus of this paper, which is the α_s^3 coefficient of the $H \to b\bar{b}$ partial width,

$$\Gamma_{H \to jj}^{(3)} = \delta\Gamma_{H \to jj}^{C_2^2,(3)} + \delta\Gamma_{H \to jj}^{C_2 C_1,(1)} + \delta\Gamma_{H \to jj}^{C_1^2} + \delta\Gamma_{H \to jj}^{\Delta_F^{(2)},(1)} + \delta\Gamma_{H \to jj}^{\Delta_F^{(3)}} + \delta\Gamma_{H \to jj}^{\Delta_H^{(1)}} \qquad (2.34)$$

The coefficient $\delta\Gamma_{H \to jj}^{C_2^2,(3)}$ has by far the most intricate IR structure, with an expansion up to the triple-real phase-space with $H \to 5$ partons. It was studied in detail in ref. [30] (in the massless approximation) and for brevity we do not provide an expansion of this term here. The remaining terms in eq. (2.34) have not yet been fully computed (and implemented into a fully flexible Monte Carlo code), however we note that the most technically complex part of the remaining pieces, corresponding to the two-loop EFT amplitudes were recently computed in ref. [37]. The results presented in this paper, combined with those presented in ref. [30] allow for a complete differential prediction for $H \to jj$ at $\mathcal{O}(\alpha_s^3)$ up to (suppressed) mass-effects in the $\delta\Gamma_{H \to jj}^{C_2^2,(3)}$ term (and presumed small top-quark mass effects missed by the EFT). Let us investigate the remaining terms in eq. (2.34) in more detail, firstly we have the "NLO" correction to the mixed $C_2 C_1$ term which appeared in the α_s^2 coefficient,

$$\delta\Gamma_{H \to jj}^{C_2 C_1,(1)} = \frac{(C_2^0 C_1^0)}{2m_H} \bigg(\int 2\text{Re}(\tilde{\mathcal{A}}_{b\bar{b},C_2}^{(0)\dagger} \tilde{\mathcal{A}}_{b\bar{b},C_1}^{(2)} + \tilde{\mathcal{A}}_{b\bar{b},C_2}^{(1)\dagger} \tilde{\mathcal{A}}_{b\bar{b},C_1}^{(1)}) F_2^2(\Phi_2) d\Phi_2$$
$$+ \int 2\text{Re}(\tilde{\mathcal{A}}_{b\bar{b}g,C_2}^{(0)\dagger} \tilde{\mathcal{A}}_{b\bar{b}g,C_1}^{(1)} + \tilde{\mathcal{A}}_{b\bar{b}g,C_2}^{(1)\dagger} \tilde{\mathcal{A}}_{b\bar{b}g,C_1}^{(0)}) F_3^2(\Phi_3) d\Phi_3$$
$$+ \sum_{ff=gg,q\bar{q}} \int 2\text{Re}(\tilde{\mathcal{A}}_{b\bar{b}ff,C_2}^{(0)\dagger} \tilde{\mathcal{A}}_{b\bar{b}ff,C_1}^{(0)}) F_4^2(\Phi_4) d\Phi_4$$
$$+ \int 2\text{Re}(\tilde{\mathcal{A}}_{b\bar{b}b\bar{b},C_2}^{(0)\dagger} \tilde{\mathcal{A}}_{b\bar{b}b\bar{b},C_1}^{(0)}) F_4^2(\Phi_4^m) d\Phi_4^m \bigg). \qquad (2.35)$$

At α_s^3, a term which is not proportional to C_2^0 appears for the first time,

$$\delta\Gamma_{H\to jj}^{C_1^2} = \frac{(C_1^0)^2}{2m_H}\left(\int|\tilde{\mathcal{A}}_{b\bar{b}g,C_1}^{(0)}|^2 F_3^2(\Phi_3)d\Phi_3\right). \tag{2.36}$$

Finally, terms arising from matching the EFT to the SM are defined as follows,

$$\delta\Gamma_{H\to jj}^{\Delta_F^{(2)},(1)} = \left(\frac{\alpha_s}{\pi}\right)^2 \Delta_F^{(2)}\Gamma_{H\to jj}^{(1)} \tag{2.37}$$

$$\delta\Gamma_{H\to jj}^{\Delta_F^{(3)}} = \left(\frac{\alpha_s}{\pi}\right)^3 \Delta_F^{(3)}\Gamma_{H\to jj}^{(0)} \tag{2.38}$$

$$\delta\Gamma_{H\to jj}^{\Delta_H^{(1)}} = \left(\frac{\alpha_s}{\pi}\right)\Delta_H^{(1)}\delta\Gamma_{H\to jj}^{C_2C_1,(0)}. \tag{2.39}$$

We note that each term here is individually $\mathcal{O}(\alpha_s^3)$ and the prefactor is related to the expansion in terms of Δ_F and Δ_H.

2.4 IR divergences

For a suitably-inclusive definition of the measurement function appearing in the previous equations, the (total) partial widths defined are IR finite. However, care must be taken if more differential quantities are considered, since the individual phase-space terms can exhibit singularities which only cancel upon integration over the unresolved regions of phase-space. In eq. (2.34) the following terms contain individual pieces which are IR divergent, $\delta\Gamma_{H\to jj}^{C_2^2,(3)}$, $\delta\Gamma_{H\to jj}^{C_2C_1,(1)}$ and $\delta\Gamma_{H\to jj}^{\Delta_F^{(2)},(1)}$. Whereas, $\delta\Gamma_{H\to jj}^{C_1^2}$, $\delta\Gamma_{H\to jj}^{\Delta_F^{(3)}}$, and $\delta\Gamma_{H\to jj}^{\Delta_H^{(1)}}$ are IR finite in all phase-space configurations. As mentioned previously, of the IR sensitive terms, $\delta\Gamma_{H\to jj}^{C_2^2,(3)}$ is by far the most complicated since it exhibits triple unresolved limits. In ref. [30] (for massless b quarks) these limits where regulated using a combination of the projection-to-Born technique [38], N-jettiness slicing [39, 40], and Catani-Seymour dipole subtraction [41]. Combined with the results for the fully inclusive width at this order [21] allowed for the construction of a fully-differential Monte Carlo code. In this paper only $\delta\Gamma_{H\to jj}^{C_2C_1,(1)}$ and $\delta\Gamma_{H\to jj}^{\Delta_F^{\text{LO}},(1)}$ require IR regulation. Both of these terms have the same singular structure as a traditional NLO calculation, although $\delta\Gamma_{H\to jj}^{C_2C_1,(1)}$ is complicated by the presence of two different "LO" terms, and as a result different pieces have different factorization properties. Since the structure is similar to a NLO calculation, we use Catani-Seymour dipoles, extended to include massive partons [42, 43]. In order to make our

predictions fully-differential in all IR-safe observables we modify $\delta\Gamma_{H\to jj}^{C_2 C_1,(1)}$ as follows,

$$
\begin{aligned}
\delta\Gamma_{H\to jj}^{C_2 C_1,(1)} = \frac{(C_2^0 C_1^0)}{2m_H}\Bigg(& \int \Big\{ 2\mathrm{Re}\left(\tilde{\mathcal{A}}_{b\bar{b},C_2}^{(0)\dagger}\tilde{\mathcal{A}}_{b\bar{b},C_1}^{(2)} + \tilde{\mathcal{A}}_{b\bar{b},C_2}^{(1)\dagger}\tilde{\mathcal{A}}_{b\bar{b},C_1}^{(1)}\right) \\
& +2\sum_{ij}\tilde{D}_{ij}\times\mathrm{Re}\left(\tilde{\mathcal{A}}_{b\bar{b},C_2}^{(0)\dagger}\tilde{\mathcal{A}}_{b\bar{b},C_1}^{(1)}\right) \Big\} F_2^2(\Phi_2)d\Phi_2 \\
& +\int\Big\{ 2\mathrm{Re}(\tilde{\mathcal{A}}_{b\bar{b}g,C_2}^{(0)\dagger}\tilde{\mathcal{A}}_{b\bar{b}g,C_1}^{(1)} + \tilde{\mathcal{A}}_{b\bar{b}g,C_2}^{(1)\dagger}\tilde{\mathcal{A}}_{b\bar{b}g,C_1}^{(0)})F_3^2(\Phi_3) \\
& \quad + 2\sum_{ij}\tilde{D}_{ij}\times\mathrm{Re}\left(\tilde{\mathcal{A}}_{b\bar{b}g,C_2}^{(0)\dagger}\tilde{\mathcal{A}}_{b\bar{b}g,C_1}^{(0)}\right)F_3^2(\Phi_3) \\
& \quad - 2\sum_{i,j,k}D_{i,j,k}(\Phi_{ijk})\times\mathrm{Re}\left(\tilde{\mathcal{A}}_{b\bar{b},C_2}^{(0)\dagger}\tilde{\mathcal{A}}_{b\bar{b},C_1}^{(1)}\right)F_2^2(\hat{\Phi}_2)\Big\}d\Phi_3 \\
& +\Big\{ \int 2\sum_{ff=gg,\,q\bar{q}}\mathrm{Re}(\tilde{\mathcal{A}}_{b\bar{b}ff,C_2}^{(0)\dagger}\tilde{\mathcal{A}}_{b\bar{b}ff,C_1}^{(0)})F_4^2(\Phi_4) \\
& \quad - 2\sum_{i,j,k}\Big[D_{i,j,k}(\Phi_{ijk})\times\mathrm{Re}\left(\tilde{\mathcal{A}}_{b\bar{b}g,C_2}^{(0)\dagger}\tilde{\mathcal{A}}_{b\bar{b}g,C_1}^{(0)}\right) \\
& \qquad\qquad + D_{i,j,k}^z(\Phi_{ijk})\times\mathrm{Re}\left(\tilde{\mathcal{A}}_{b\bar{b}n,C_2}^{(0)\dagger}\tilde{\mathcal{A}}_{b\bar{b}n,C_1}^{(0)}\right)\Big]F_3^2(\hat{\Phi}_3)\Big\}d\Phi_4 \\
& +\int 2\mathrm{Re}(\tilde{\mathcal{A}}_{b\bar{b}b\bar{b},C_2}^{(0)\dagger}\tilde{\mathcal{A}}_{b\bar{b}b\bar{b},C_1}^{(0)})F_4^2(\Phi_4^m)d\Phi_4^m \Bigg).
\end{aligned} \tag{2.40}
$$

In eq. (2.40) the subtraction terms are defined by $D_{i,j,k}(\Phi_{ijk})$ where $\Phi_{ijk}=\{p_i,p_j,p_k\}$ defines the emitter, emitted and spectator partons and $\hat{\Phi}$ defines the mapped phase-space used in the lower order subtraction (and relevant measurement function). Integrating the dipoles over the dipole phase-space generates the integrated dipole terms $\tilde{D}_{ij}$. Due to the low total number of total partons, color conservation simplifies the color correlations $\mathbf{T}_i\cdot\mathbf{T}_j$ to the level of overall multiplicative factors. However spin correlations in $g\to gg$ and $g\to q\bar{q}$ splitting require care, and are regulated additionally by the azimuthal terms $D_{i,j,k}^z$ (see ref. [42] for further details), which require modified tree-level amplitudes $\tilde{\mathcal{A}}_{b\bar{b}n,C_i}^{(0)}$ with the gluon polarization vector replaced by the spin-reference vector n. In eq. (2.40) the IR structure of the two-body and four-body phase-space is self-evident, the two-body phase-space only has explicit poles in ϵ, which are directly canceled by the integrated terms arising from the tree-body subtraction term. The four-body phase-space only has implicit poles which arise upon integration over the unresolved regions of phase-space. These are compensated by the subtraction terms on the seventh and eighth lines of the formula. The three-body phase-space is more complicated since it requires regulation of both types of term. The fourth line corresponds to the integrated subtractions of the four-body phase-space, these cancel the explicit poles in ϵ which reside in both $\tilde{\mathcal{A}}_{b\bar{b}g,C_2}^{(0)\dagger}\tilde{\mathcal{A}}_{b\bar{b}g,C_1}^{(1)}$ and $\tilde{\mathcal{A}}_{b\bar{b}g,C_2}^{(1)\dagger}\tilde{\mathcal{A}}_{b\bar{b}g,C_1}^{(0)}$. The fifth line in eq. (2.40) defines the counter-terms required to cancel the implicit poles in the (ϵ^0) part of $\tilde{\mathcal{A}}_{b\bar{b}g,C_2}^{(0)\dagger}\tilde{\mathcal{A}}_{b\bar{b}g,C_1}^{(1)}$ (which we recall corresponds to the one-loop EFT amplitude interfered with the tree-level $H\to b\bar{b}g$). The other term $\tilde{\mathcal{A}}_{b\bar{b}g,C_2}^{(1)\dagger}\tilde{\mathcal{A}}_{b\bar{b}g,C_1}^{(0)}$ which corresponds
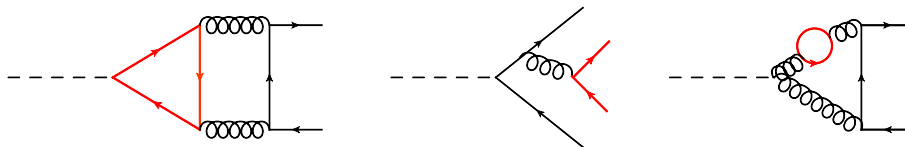
Figure 4. Additional contributions which can arise in $H \to c\bar{c}$ with the addition of a second active heavy quark (bottom) shown in red.

to a tree-level EFT amplitude interfered with a one-loop $H \to b\bar{b}g$ amplitude (in which the Higgs couples directly to the b quarks) is finite in the limit $p_g \to 0$. This can be seen since although the one-loop amplitude exhibits soft singular behaviour, it is sufficiently damped by the EFT tree (which requires a hard emission) to avoid any further singular behavior.

The IR behaviour of $\delta\Gamma_{H\to jj}^{\Delta_F^{(2)},(1)}$ is exactly that of the NLO computation of the partial width and can be readily expressed in terms of the dipole functions listed above. For brevity we do not provide the result here.

2.5 Calculation methodologies

All amplitudes calculated in this publication were generated with QGraf [44] and then interfered with each other to obtain the relevant squared amplitudes. Traces were computed with TRACER [45] and the resulting integrals reduced to master integrals with the help of integration-by-parts identities generated by LiteRed [46, 47] and Reduze [48]. The expressions for the relevant two-loop master integrals have been presented in [49, 50], where required, one-loop integrals were evaluated numerically using QCDLoop [51, 52].

2.6 Additional master integrals for $H \to c\bar{c}$

Thus far, the discussion in this section has specifically related to the computation of $H \to b\bar{b}$. The calculation can, however, be readily extended to include the decay $H \to c\bar{c}$. The primary difference when considering charm quarks is that there are now two active massive flavors (charm and bottom quarks). The vast majority of the calculation can simply be obtained from the results in this section with the replacements $b \to c$, $m_b \to m_c$ and $y_b \to y_c$. We also define the replacement $C_2 \to C_3$ (this is purely for later notational convenience $C_3 = C_2$). This leaves contributions which are dependent on the bottom and charm quark simultaneously. Example topologies are shown in figure 4. We see there are three basic types of additional corrections. Firstly there are two body contributions which are proportional to $y_b y_c$, while a second type of term contains the four-quark amplitude $H \to b\bar{b}c\bar{c}$. Depending on which quark line the Higgs couples to, the resultant matrix element squared can be proportional to either y_c^2, $y_b y_c$ or y_b^2. There is therefore some ambiguity as to whether these pieces are included in $H \to b\bar{b}$ or $H \to c\bar{c}$ (or both). In our computation of $H \to b\bar{b}$ we take $m_c = 0$ and these terms enter as part of the double-real NNLO correction (keeping the y_b^2 term only). In our computation of $H \to c\bar{c}$ we include all three types of contribution as a component of the partial width. These y_b sensitive pieces, which occur at $\mathcal{O}(\alpha_s^2)$ are therefore included in our calculation. However, their impact will be shown to be small, as such we do not compute the $\mathcal{O}(\alpha_s^3)$ correction to these processes in

this paper. A final type of diagram, which also occurs at $\mathcal{O}(\alpha_s^3)$, is also shown in figure 4. This term induces an m_b dependence into the EFT-y_c piece.

The new loop amplitudes discussed above require 20 new additional master integrals (MI's). These integrals have been computed for the case of bottom-top loops in [33], however the results are not fully public.[2] In this work we have reproduced the calculation, using the method of differential equations [55–58] and have included the results as supplementary material as well as in the `arXiv` submission. We outline the details of the computation in the remainder of this section, while enthusiastic readers can find further technical details in appendix B. We define the kinematics of the process as follows, $H(p_H) \to c(p_1) + \bar{c}(p_2)$ where $p_1^2 = p_2^2 = m_c^2$ and $p_H^2 = m_H^2$. The additional master integrals can be expressed in terms of the following integral family

$$\mathcal{I}(n_1, \ldots, n_7) = \left(\frac{1}{\Gamma(1+\epsilon)}\right)^2 \left(\frac{\mu^2}{m_b^2}\right)^{2\epsilon} \int \frac{d^D k_1}{(i\pi)^{D/2}} \frac{d^D k_2}{(i\pi)^{D/2}} \frac{1}{D_1^{n_1} \ldots D_7^{n_7}}, \qquad (2.41)$$

with the dimensional regularization parameter $\epsilon = \frac{D-4}{2}$ and the propagators defined as

$$D_1 = k_1^2 - m_c^2, \quad D_2 = k_2^2 - m_b^2, \qquad D_3 = (k_1 + p_1)^2, \quad D_4 = (k_1 - k_2 + p_1)^2 - m_b^2,$$
$$D_5 = (k_1 - p_2)^2, \quad D_6 = (k_2 - p_H)^2 - m_b^2, \quad D_7 = (k_2 + p_1)^2. \qquad (2.42)$$

It is further convenient to introduce the following dimensionless variables

$$-\frac{m_H^2}{m_b^2} = \frac{(1-w^2)^2}{w^2}, \quad \frac{m_c^2}{m_b^2} = \frac{(1-w^2)^2 z^2}{(1-z^2)^2 w^2}. \qquad (2.43)$$

In order to determine the MI's we use the Magnus algorithm [59, 60] which allows us to identify a particular set of integrals defined in (B.1), which satisfy a canonical differential equation

$$d\vec{\mathrm{I}} = \epsilon \sum_{i=1}^{12} \mathbb{M}_i d\log(\eta_i) \vec{\mathrm{I}}. \qquad (2.44)$$

Here $\mathbb{M}_i$ is a 20×20 matrix of rational numbers. For a canonical differential equation the dimensional regularization parameter ϵ has factorized from the kinematics, which are encoded in a $d\log$-form. The arguments of these $d\log$'s are called letters, and taken together they form the alphabet of our problem

$$\begin{aligned}
\eta_1 &= 1 - w, & \eta_2 &= w, & \eta_3 &= 1 + w, & \eta_4 &= 1 + w^2, \\
\eta_5 &= 1 - z, & \eta_6 &= z, & \eta_7 &= 1 + z, & \eta_8 &= 1 + z^2, \\
\eta_9 &= w - z, & \eta_{10} &= w + z, & \eta_{11} &= 1 - wz, & \eta_{12} &= 1 + wz.
\end{aligned} \qquad (2.45)$$

Since all letters in our alphabet exhibit algebraic roots, the solution of the differential equation can be expressed in terms of generalized polylogartihms [61–64]. To complete the solutions of the differential equations a boundary constant has to be specified. In our case demanding the regularity of our solutions at the pseudothreshold $m_H^2 = 0$ provides relations

---

[2]See also refs. [53, 54] for a discussion of cases with one nonzero mass.

	Partial Width [MeV]	$\mu = m_H/2$	$\mu = m_H$	$\mu = 2m_H$
$\mathcal{O}(\alpha_s^0)$	$\Gamma_{H \to jj}^{(0)}$	2.1599	1.9180	1.7246
$\mathcal{O}(\alpha_s^1)$	$\Gamma_{H \to jj}^{(1)}$	0.2603	0.3989	0.4822
$\mathcal{O}(\alpha_s^2)$	$\delta\Gamma_{H \to jj}^{C_2^2}$	-0.0099	0.0732	0.1418
	$\delta\Gamma_{H \to jj}^{C_1 C_2}$	0.02656	0.02418	0.02202
$\mathcal{O}(\alpha_s^3)$	$\delta\Gamma_{H \to jj}^{C_2^2}$	-0.01514	0.00431	0.03542
	$\delta\Gamma_{H \to jj}^{C_1 C_2}$	0.00946	0.01306	0.01476
	$\delta\Gamma_{H \to jj}^{C_1^2}$	0.00920	0.00670	0.00504

Table 1. Inclusive partial width results for $H \to b\bar{b}$ at LO, and higher order coefficients for NLO y_b^2 contributions, and the top induced pieces at $\mathcal{O}(\alpha_s^2)$ and $\mathcal{O}(\alpha_s^3)$.

between the boundary constants of 17 integrals. The remaining three integrals $I_{1,2,5}$ are then taken as an independent input. Their solutions were first computed in the Euclidean region $m_H^2 < 0, m_c^2 > 0, m_b^2 > 0$ and then analytically continued to the production region $m_H^2 > 4m_c^2$ by adding a small positive imaginary part to the Higgs mass $m_H^2 \to m_H^2 + i0^+$. We have checked our solutions in both regions against their numerical expression provided by SecDec [65, 66] and found full agreement.

3 Results for $H \to b\bar{b}$

We have implemented the calculation described in the previous section into a fully flexible parton-level Monte Carlo code, based upon the structure of MCFM [67–69]. For the results presented in this paper we take the mass of the decaying Higgs boson to be $m_H = 125\,\text{GeV}$, we take $\alpha_s(m_Z) = 0.118$. We use a pole mass of $m_b = 4.78\,\text{GeV}$, and in the Yukawa coupling the $\overline{\text{MS}}$ mass of $m_b(m_H) = 2.80\,\text{GeV}$. Our remaining electroweak parameters are $G_F = 0.116638 \times 10^{-4}\,\text{GeV}^{-2}$, and $m_W = 80.385\,\text{GeV}$, and $v = 246\,\text{GeV}$.

Since we are interested in presenting results with the application of jet clustering and b-tagging, we cluster partons into jets using the Durham jet algorithm [70, 71]. This algorithm starts from a set of ordered momentum (which for us correspond to partons), and computes the following quantity y_{ij} for all pairs of objects i and j:

$$y_{ij} = \frac{2\min(E_i^2, E_j^2)(1 - \cos\theta_{ij})}{Q^2}. \tag{3.1}$$

Where E_i is the energy of object i, and θ_{ij} defines the angle between the two objects i and j. Q is the total energy of the system, which in our case is m_H. If $y_{ij} < y_{\text{cut}}$, the two objects are combined into a new one with four momentum equal to $p_i + p_j$. The procedure

is then iterated until no more clustering is possible and the resulting n final objects are classified as n jets. We work in the Higgs rest frame, although in order to define dynamic observables at LO we define the fictitious collision axis $\pm\hat{z}$ which allows us to compute rapidities and transverse momentum of jets at LO.

We begin by computing inclusive partial widths, our results are summarized in table 1. We list the coefficients of the partial width expansion up to third order. Since the primary interest of this work is the relative size of the pieces proportional to C_1 we present the following breakdown at each order (where appropriate)

$$\delta\Gamma_{H\to jj}^{C_2^2} = \begin{cases} \delta\Gamma_{H\to jj}^{C_2^2,(2)} + \delta\Gamma_{H\to jj}^{\Delta_F^{(2)},(0)} & \text{at} \quad \alpha_s^2 \\ \delta\Gamma_{H\to jj}^{C_2^2,(3)} + \delta\Gamma_{H\to jj}^{\Delta_F^{(2)},(1)} + \delta\Gamma_{H\to jj}^{\Delta_F^{(3)},(0)} & \text{at} \quad \alpha_s^3 . \end{cases} \tag{3.2}$$

These pieces define those which scale like y_b^2, on the other hand, the top sensitive pieces are grouped at each order as follows,

$$\delta\Gamma_{H\to jj}^{C_1 C_2} = \begin{cases} \delta\Gamma_{H\to jj}^{C_1 C_2,(0)} & \text{at} \quad \alpha_s^2 \\ \delta\Gamma_{H\to jj}^{C_1 C_2,(1)} + \delta\Gamma_{H\to jj}^{\Delta_H^{(1)},(1)} & \text{at} \quad \alpha_s^3 . \end{cases} \tag{3.3}$$

In the discussion in the rest of this section we will refer to these combinations as EFT-y_b pieces. At α_s^3 we also separate the contribution arising from C_1^2 (referred to subsequently as EFT^2 pieces). In the computation of the $\delta\Gamma_{H\to jj}^{C_2^2,(3)}$ and $\delta\Gamma_{H\to jj}^{C_2^2,(2)}$ contributions we take the inclusive partial width [21] with $m_b = 0$ and re-weight by the LO with the full m_b-kinematics.

Inspection of the table confirms that the mixed EFT-y_b pieces contribute around a percent to the partial width at $\mathcal{O}(\alpha_s^2)$. The main results of this paper are included in the $\mathcal{O}(\alpha_s^3)$ rows. We observe that the mixed EFT-y_b has a sizable correction at NLO (of which around $1/3$ is made up of the correction arising from the Wilson coefficient), the "LO" to "NLO" K-factor for this process is around 1.3-1.5 for the scales presented in the table. The EFT^2 contribution is of the same order as the mixed term (and y_b^2 coefficient at this order), and contributes around 0.5% to the total partial width. Rescaling $y_b = \kappa_b y_b$ and $C_1^0 = \kappa_g C_1^0$ we can write the total partial width (at $\mu = m_H$) as follows,

$$\Gamma_{H\to b\bar{b}+X}^{\text{N3LO}}[\mu = m_H] = 2.394 \times \left(\kappa_b^2 + 0.016 \times \kappa_b \kappa_g + 0.003 \times \kappa_g^2\right) + \mathcal{O}(\alpha_s^4) \quad \text{MeV} \tag{3.4}$$

Thus the effects of having $\kappa_g \neq 0$ in the above equation change the extraction of the partial width by around 2%. Given the intricate phase-space of these terms we expect that there is a strong sensitivity to jet-clustering and selection criteria which may be employed in an experimental analysis. We investigate this in the next section.

3.1 Differential predictions for $H \to b\bar{b}$

In the last section we presented results for the EFT contributions to the inclusive width at $\mathcal{O}(\alpha_s^3)$, of course, the primary advantage of our calculation is the ability to employ arbitrary jet clustering and cuts to the decay products. Indeed, the impact of the EFT initiated pieces are expected to be very sensitive to the precise nature of the final state selection cuts. This

can already been seen at the $\mathcal{O}(\alpha_s^2)$ level, approximately 80% of the mixed $C_1 C_2$ coefficient arises from the 3-body decay channel. Therefore any selection requirement which eliminates 3-jet topologies (for instance running the Durham-jet algorithm with a small y_{cut}, so that more events are classified as three-jet events, then asking for $H \to jj$) will dramatically curtail the contribution from the mixed pieces. A further sensitivity to the final state definition arises through the application of b-tagging. Since the EFT contributions produce the final state bottom quarks through $g \to b\bar{b}$ splitting, many favorable phase-space configurations will result in jets with both b and $\bar{b}$ partons placed in the same jet. Therefore requiring two resolved b-jets will damp the interference terms. With these points in mind we therefore compare predictions with the following three jet clustering requirements:

- No veto on additional jets

- Requiring exactly two jets

- Requiring exactly two b-jets.

We take $y_{\mathrm{cut}} = 0.1$ as a representative jet clustering choice (assuming these jets are somewhat similar to an anti-k_T jet with $p_T \sim y_{cut} m_H$). Since we retain the mass of the bottom quark throughout we are able to classify jets containing a $b\bar{b}$ pair as $b-$tagged. However, as mentioned before, requiring two b-tags effectively vetoes these configurations such that differences arising from the treatment of $g \to b\bar{b}$ (which can be troublesome for massless calculations) are of limited concern here.

In figure 5 we present the transverse momentum of the leading jet with respect to the fictitious collision axis, rescaled by the Higgs mass m_H. The uppermost part of the figure presents differential predictions for the total NLO partial width combined with the mixed EFT-y_b pieces at NLO and the EFT^2 pieces. The lower panels show the relative impact of these new pieces compared to the basic NLO prediction. We present results for fully inclusive predictions $H \to jj + X$ (green), requiring exactly two jets $H \to jj$ (blue) and finally requiring exactly two b-tagged jets (red). The upper most ratio-plot compares the $\mathcal{O}(\alpha_s^2)$ mixed EFT$-y_b$ to the NLO y_b^2 baseline. We note that in each ratio we divide by the NLO evaluated at the same scale as the numerator, and impose the final state phase-space cuts on the numerator and denominator in both instances. In all three jet configurations we observe a reasonably flat correction, the size of which is sensitive to the jet requirements. At this order, the dominance of the 3-body phase-space topology can be seen by the dramatic reduction as the inclusive phase-space is reduced to the 2-jet topology. The $\mathcal{O}(\alpha_s^2)$ mixed EFT$-y_b$ terms are reduced from around a 1% effect inclusively to 0.3% when two-jets are mandated. Further b-tagging results in very little difference with respect to the two-jet predictions.

The middle ratio panel presents the NLO predictions for the mixed EFT$-y_b$, (again with respect to the NLO y_b^2 pieces with equivalent cuts applied). Inclusively we see the impact of the large K factor for these predictions, especially in the lower p_T region, which has increased by around a factor of 2 to 2%. However, at NLO the mixed EFT$-y_b$ are even more sensitive to the jet requirements, after imposing the two-jet requirements we see that these pieces are reduced to around 1% of the NLO prediction. Demanding two b jets further suppresses the impact of the NLO mixed EFT-y_b pieces, by an additional factor of two such that they contribute around 0.5% level across the phase-space. The
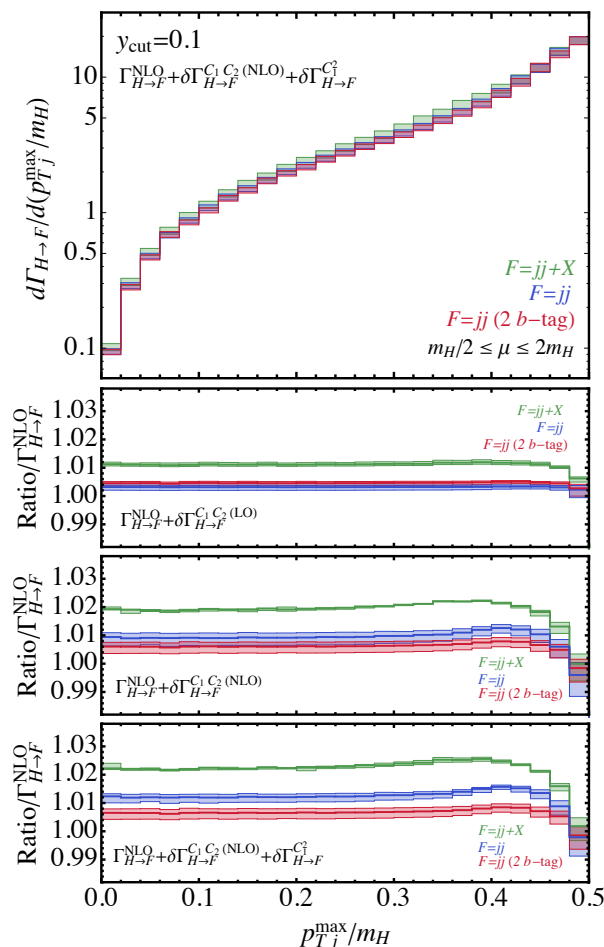
Figure 5. Differential predictions for the (fractional) transverse momentum (with respect to a fictitious collision axis $\pm\hat{z}$) of the leading jet, clustered with $y_{\text{cut}} = 0.1$. Results are presented for a variety of different requirements on the final state jets, either no restrictions $H \to jj + X$ (green), requiring exactly two jets $H \to jj$ (blue) or exactly two b-tagged jets $H \to b\bar{b}$ (red). The lower panels present the impact of the mixed EFT-y_b piece at $\mathcal{O}(\alpha_s^2)$, $\mathcal{O}(\alpha_s^3)$, and the combined EFT-y_b and EFT^2 piece at $\mathcal{O}(\alpha_s^3)$, with respect to the NLO y_b^2 prediction.

bottom panel presents the combined NLO mixed EFT$-y_b$ piece and EFT^2 contribution. The inclusion of the EFT^2 piece increases the inclusive and $H \to jj$ pieces by around 0.3%, but is significantly suppressed by demanding two b-jets. This is anticipated since here the phase-space strongly favors the quasi-collinear limit arising from gluon splitting which rarely results in two b-tagged jets in the Higgs rest frame.

It is also interesting to compare the impact of these new pieces to that of the remaining $\mathcal{O}(\alpha_s^3)$ contributions. Such a comparison is made more difficult since here we have retained the mass of the bottom quark in full, whereas in ref. [30] $m_b = 0$ kinematically. In lieu of a more detailed phenomenological study, figure 7 in ref. [30] can be inspected to provide some insight. The N^{3}LO prediction for the y_b^2 pieces for this observable (for the $H \to jj$ selection criteria) is around 5% across the bulk of phase-space (with larger impacts in the $p_T \sim m_H/2$ region). The equivalent results from our calculation here correspond to the
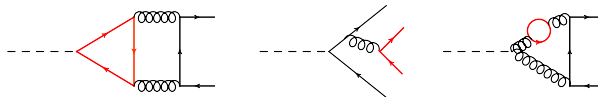
Figure 6. Differential predictions for the (m_H-scaled) energy of the leading jet, in 2-jet events defined with $y_{\rm cut} = 0.1$. Results are presented for a variety of different requirements on the final state jets, either requiring exactly two jets $H \to jj$ (blue) or exactly two b-tagged jets (red). The lower panels present the impact of the mixed EFT-y_b piece at $\mathcal{O}(\alpha_s^2)$, $\mathcal{O}(\alpha_s^3)$, and the combined EFT-y_b and EFT^2 piece at $\mathcal{O}(\alpha_s^3)$, with respect to the NLO y_b^2 prediction.

blue curve on the bottom panel, from which we learn that the EFT component of the combined $\mathcal{O}(\alpha_s^3)$ coefficient is about 20%.

In figure 6 we study the energy of the leading jet (rescaled by the Higgs mass) for two-jet events. This is a different type of observable than the p_T studied previously, as it is a delta function at LO (where each jet has an energy of $m_H/2$). As such it is more sensitive to higher order corrections since the bulk of the phase-space is one order lower in perturbation theory. Further evidence of the sensitivity of this observable to the underlying structure of the partonic phase space is manifest in this distribution around $E_j^{\rm max} \sim 0.6\,m_H$. At higher energies only the four-parton phase space topologies are capable of producing a contribution, and the observable is effectively Leading Order. For values of $E_j^{\rm max}$ less than 0.6 m_H the three- and four-parton phase space configurations contribute and the observable is effectively Next-to-Leading Order. Similar features for this observable are discussed for the other α_s^3 contributions in ref. [30]. With regards to the top induced pieces we observe a similar trend to the p_T distribution studied previously. The LO mixed EFT$-y_b$ is strongly suppressed by the application of the two-jet requirement, and is a sub-percentage effect across the phase-space. The higher order corrections to the mixed EFT-y_b term opens up a more dynamic three-parton and four-parton phase-space and results in relatively large corrections (middle ratio panel). Without specifically requiring b-tagging the contribution to the bulk of the phase-space is around 3-4%, which is reduced to around 2-3% when the b-tagging algorithm is applied. The $H \to jj$ rate is increased by around 0.5-1% by the inclusion of the EFT^2 contribution, but this again is significantly reduced by the requirement of two b-tags. Finally comparison with figure 8, in ref. [30] shows that the EFT initiated effects are rather small compared to the total impact of the other α_s^3 pieces with bulk corrections around 30-50% for the combined α_s^2 and α_s^3 coefficient. We note however, that although these residual EFT effects are small ($\sim$10% of the total α_s^3 contribution), their magnitude is comparable to, or larger than, the scale uncertainty at this order. The far tail in this distribution is only directly accessible by the four-parton contribution (which exists in the NLO correction to the mixed EFT-y_b pieces), and a comparison with the NLO partial width is not valid.

Summarizing, in this section we have presented a short study of the EFT initiated pieces at $\mathcal{O}(\alpha_s^3)$. We found that the impact of these pieces is sensitive to the nature of the final state selection cuts. This is hardly surprising, given that this contribution arises from an interference of two disparate phase-spaces. The pure-EFT diagrams are largest when the $g \to b\bar{b}$ splitting is quasi-collinear which suppresses the two b-jet rate significantly.

	Partial Width [MeV]	$\mu = m_H/2$	$\mu = m_H$	$\mu = 2m_H$
$\mathcal{O}(\alpha_s^0)$	$\Gamma_{H\to c\bar{c}}^{(0)}$	0.1047	0.0930	0.0836
$\mathcal{O}(\alpha_s^1)$	$\Gamma_{H\to c\bar{c}}^{(1)}$	0.0122	0.0190	0.0231
$\mathcal{O}(\alpha_s^2)$	$\delta\Gamma_{H\to c\bar{c}}^{C_3^2},\ [y_c^2]$	-0.0005	0.0035	0.0069
	$\delta\Gamma_{H\to c\bar{c}}^{C_1 C_3}\ [\text{EFT-}y_c]$	0.0036	0.0030	0.0026
	$\delta\Gamma_{H\to c\bar{c}}^{C_2 C_3}\ [y_b y_c]$	0.0001	0.00007	0.00005
	$\delta\Gamma_{H\to c\bar{c}}^{C_2^2}\ [y_b^2]$	$\sim 10^{-6}$	$\sim 10^{-6}$	$\sim 10^{-6}$
$\mathcal{O}(\alpha_s^3)$	$\delta\Gamma_{H\to c\bar{c}}^{C_3^2}\ [y_c^2]$	-0.0008	0.0002	0.0017
	$\delta\Gamma_{H\to c\bar{c}}^{C_1 C_3}\ [\text{EFT-}y_c]$	0.0020	0.0023	0.0023
	$\delta\Gamma_{H\to c\bar{c}}^{C_1^2}\ [\text{EFT}^2]$	0.0154	0.0112	0.0084

Table 2. Inclusive partial width results for $H \to c\bar{c}$ at LO, and higher order coefficients for NLO y_c^2 contributions, and the top induced pieces at $\mathcal{O}(\alpha_s^2)$ and $\mathcal{O}(\alpha_s^3)$.

Therefore the impact of these pieces varies from a few precent (and hence crucial for future precision studies), to sub-percent (and less relevant to phenomenology) depending on the specific final state selection criteria employed. It is difficult to speculate on LHC applications given that we have used the Durham jet algorithm in the Higgs rest-frame, but its seems reasonable to postulate that analysis which require two resolved b-jets will have very small impacts from the EFT initiated pieces, whereas those that include boosted jets include more of the $g \to b\bar{b}$ splitting pieces and are more sensitive to the EFT pieces. However, the uncertainties with this type of analysis are rather large and unlikely to be at the percent level in the near future. In the longer term, final studies at the HL-LHC and proposed FC analyses aiming for precent precision accuracy should carefully model these pieces.

4 Results for $H \to c\bar{c}$

4.1 Inclusive results

In this section we present an analysis of the $H \to c\bar{c}$ decay. We use a charm pole mass of $m_c = 1.67\,\text{GeV}$ which is used in the kinematics and propagators, in the Yukawa coupling we use $m_c^{\overline{\text{MS}}} = \{0.65, 0.61, 0.58\}\,\text{GeV}$ at the scales $\{0.5, 1, 2\} \times m_H$ respectively. All other parameters are the same as defined in our computations of $H \to b\bar{b}$.

In table 2 we present a summary of the inclusive contributions to final states involving charm-quarks. From a comparison with the equivalent table for bottom quarks (table 1) we see that the relative impact for the EFT pieces is much larger for charm quarks. Taking $\mu = m_H$ as a reference point we see that for the charm decays the EFT-y_c piece is the same

size as the y_c^2 correction at $\mathcal{O}(\alpha_s^2)$, and a factor of 10 bigger at $\mathcal{O}(\alpha_s^3)$. For comparison the same ratios for $H \to b\bar{b}$ are approximately 33% and three. The relative enhancements come from two sources. For a given quark species f, the overall scaling of the mixed-EFT terms to the LO behaves like,

$$\frac{y_f m_f}{y_f^2} \propto \frac{m_f}{m_f^{\overline{\text{MS}}}(m_H)} \tag{4.1}$$

which is equal to around 2.5 for charm quarks and 1.67 for bottoms. Thus the mixed terms are relatively more important for the charm quarks. Secondly, the smaller charm mass causes a larger quasi-collinear enhancement of the $g \to c\bar{c}$ splitting (compared to $g \to b\bar{b}$) which increases the importance of the EFT amplitude. However, there is a difference with respect to the bottom quark, for charm's there is a destructive interference between the two-body phase-space and the three-body phase-space at LO. This destructive interference is also present at NLO, but the inclusion of additional positive contributions from the four-body phase-space conspire to produce a rather sizable K-factor $(1.5 - 2)$ in going to NLO in the mixed EFT-y_c pieces.

A new feature of the $H \to c\bar{c}$ partial widths is the $y_b y_c$ mixed term and y_b^2 term which appear at $\mathcal{O}(\alpha_s^2)$. As discussed in section 2 there is an ambiguity as to whether one includes these contributions in either the $H \to b\bar{b}$ or $H \to c\bar{c}$ partial widths. In our setup it makes most sense to include them in the discussion of $H \to c\bar{c}$, since $m_c = 0$ in our $H \to b\bar{b}$ and accordingly these terms either vanish or are IR-unsafe in isolation. Either way, it is clear from the results in table 2 that these pieces are rather small and unless targeted with a particularly exotic experimental selection requirement, are of limited phenomenological relevance. The y_b^2 term, corresponding to the four-quark amplitudes interfering at tree-level is very small $(\sim 1\,\text{eV})$, the mixed $y_b y_c$ is dominated by the 2-body term. Given the smallness at $\mathcal{O}(\alpha_s^2)$, and its technical complexity, we do not study these terms at $\mathcal{O}(\alpha_s^3)$. Table 2 also highlights the large impact of the EFT^2 contributions to the inclusive width. At around 10% of the LO partial width, these pieces dominate all corrections beyond NLO in the expansion. Their increase in relative importance is because they do not suffer any suppression when moving from bottom to charm quarks in the final state, and are in fact enhanced by the increased effect of the quasi-collinear splitting due to smaller charm quark mass $(\log(m_b^2/m_c^2) \sim 2)$. For the $H \to b\bar{b}$ decay we observed a strong sensitivity to jet selection criteria for these pieces, therefore in the next subsection we will turn our attention to a differential analysis.

4.2 Differential predictions for EFT-induced contributions to $H \to c\bar{c}$

In this section we compute differential predictions for $H \to c\bar{c}$, again focussing on the pieces arising from the EFT contributions at NLO. As in the analysis for $H \to b\bar{b}$ we use the Durham jet algorithm with $y_{\text{cut}} = 0.1$, we compute the transverse momentum and energy (rescaled by the Higgs mass) for the leading jet in 2-jet and 2 $c-$tagged jet selection cuts. Our results are shown for the transverse momentum in figure 7, and energy in figure 8. As before the upper panel shows the differential distribution, and the lower panels present various ratios to the respective NLO predictions (with the selection cuts applied). Focusing first on the transverse momentum, inspection of the lower panels shows that the
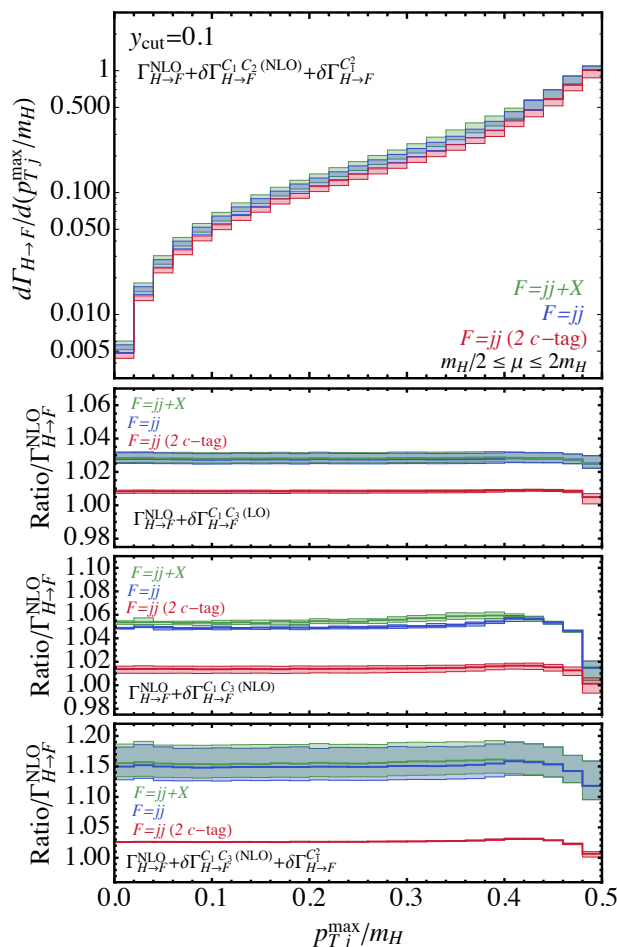
Figure 7. Differential predictions for the (fractional) transverse momentum (with respect to a fictitious collision axis $\pm\hat{z}$) of the leading jet, clustered with $y_{\text{cut}} = 0.1$. Results are presented for a variety of different requirements on the final state jets, either no restrictions $H \to jj + X$ (green), requiring exactly two jets $H \to jj$ (blue) or exactly two c-tagged jets (red). The lower panels present the impact of the mixed EFT-y_c piece at $\mathcal{O}(\alpha_s^2)$, $\mathcal{O}(\alpha_s^3)$, and the combined EFT-y_c and EFT^2 piece at $\mathcal{O}(\alpha_s^3)$, with respect to the NLO y_c^2 prediction evaluated with the same cuts.

mixed EFT-y_c terms at NLO correspond to around a 5% correction across the bulk of the distribution, but are again significantly reduced by demanding exactly two c-tagged jets in the final state. The bottom panel highlights the huge impact of the EFT^2 contribution inclusively, around 15%. However, once again, the requirement that the two charm quarks reside in different tagged jets significantly damps the relative importance of the contribution. The total EFT sensitive pieces (mixed + squared) contribute around the 2-3% of the NLO if two c-jets are required. A similar story is shown in the energy distribution, across the bulk of the phase-space only the 3- and 4-body phase-space configurations contribute, resulting in a larger relative impact of the EFT pieces. Again, application of a charm tagging algorithm significantly reduces these contributions, by around a factor of four.
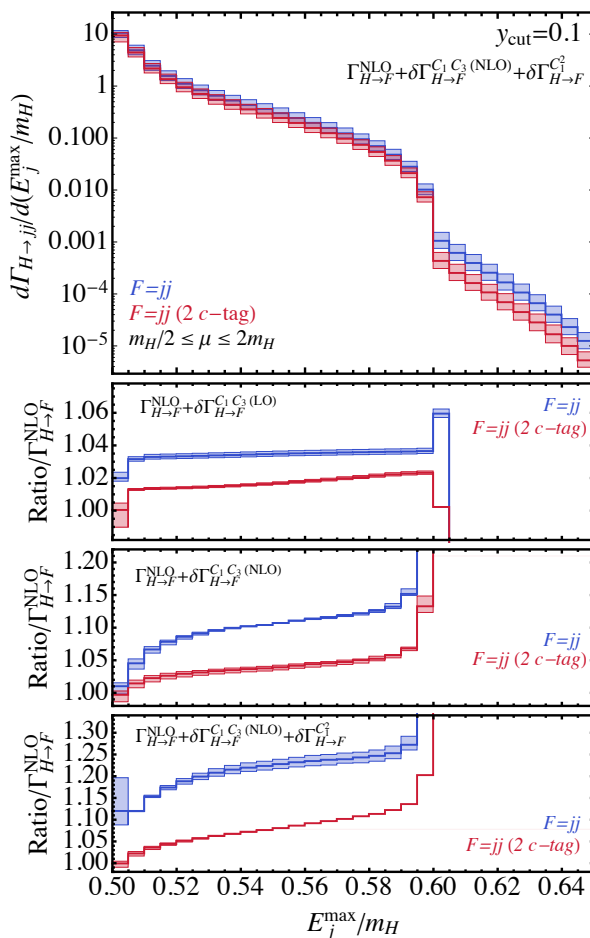
Figure 8. Differential predictions for the (m_H-scaled) energy of the leading jet in 2-jet events (in $H \to c\bar{c}$ decays) defined with $y_{\mathrm{cut}} = 0.1$. Results are presented for a variety of different requirements on the final-state jets, either requiring exactly two jets $H \to jj$ (blue) or exactly two c-tagged jets (red). The lower panels present the impact of the mixed EFT-y_c piece at $\mathcal{O}(\alpha_s^2)$ and $\mathcal{O}(\alpha_s^3)$, and the combined EFT-y_c and EFT^2 pieces at $\mathcal{O}(\alpha_s^3)$, with respect to the NLO y_c^2 prediction.

4.3 Impact on LHC (and FC) studies of $H \to c\bar{c}$

Finally, we conclude this section with a brief comment regarding the impact of the EFT induced pieces on $H \to c\bar{c}$ measurements at the LHC. Summing the contributions in table 2 and rescaling $y_c = \kappa_c y_c$ and $C_1^0 = \kappa_g C_1^0$ (i.e. each κ_X picks out the pure-charm and pure-EFT amplitudes, and $\kappa_X = 1$ in the SM) we can write

$$\Gamma_{H \to c\bar{c}+X}^{\mathrm{N3LO}}[\mu = m_H] = 0.0967 \left(\kappa_c^2 + 0.055 \times \kappa_c \kappa_g + 0.116 \times \kappa_g^2 \right) + \mathcal{O}(\alpha_s^4) \quad \mathrm{MeV} \quad (4.2)$$

Thus there is room for a significant mismeasurement ($\sim 15\%$) of κ_c if $\kappa_g = 0$ is enforced in the above equation. One should therefore ensure that these pieces are adequately modeled if an extraction of y_c is attempted at a level of 20% or better. As a rule of thumb analyses which are sensitive to $g \to c\bar{c}$ splittings will have a large impact from κ_g pieces. For example, requiring two isolated charm-tagged jets will likely reduce the contributions down to the

level of a few percent, whereas analyses that allow QCD radiation to fall into the same jet (e.g. boosted) searches, will be more exposed to this type of correction. Interestingly, both types of analysis are currently employed in the experimental analyses [12]. We leave a more detailed LHC phenomenological study to a future publication.

5 Conclusions

In this paper we have presented a calculation of the EFT-sensitive pieces arising in $H \to q\bar{q}$ decays at $\mathcal{O}(\alpha_s^3)$. We have retained the mass of the final-state quarks throughout our calculation, and worked in an EFT in which the top quark is integrated out of the theory. This calculation required the computation of the two-loop amplitudes in the EFT interfered with the tree-level $H \to q\bar{q}$ amplitude and the one-loop corrections in the EFT interfered with the one-loop corrections to $H \to q\bar{q}$ (2-body phase-space contributions). The three-body phase-space consisted of a one-loop EFT (or y_q) $H \to q\bar{q}g$ amplitude interfered with the y_q (or EFT) tree-level amplitude. Finally, there are four-body terms which are tree-level four-parton amplitudes in the EFT interfered with those proportional to y_q.

These EFT-induced pieces are computationally interesting, since the $\mathcal{O}(\alpha_s^2)$ amplitudes are UV divergent, but IR-finite. Our computation therefore bears some hall-marks of an NLO computation and some of an NNLO computation in QCD. The three contributing phase-space regions act like double-virtual, real-virtual, and double-real terms in a traditional NNLO calculation, but they can be regulated using a NLO dipole subtraction setup. The UV renormalization at this order is intricate, especially given the mixed renormalization scheme employed, in which the Yukawa coupling is renormalized in the $\overline{\text{MS}}$ scheme while the bottom quark mass is renormalized in the on-shell scheme. As a result, the amplitudes scale like $y_q^{\overline{\text{MS}}} m_q^{\text{OS}}$.

We implemented our results into a Monte Carlo code (based upon MCFM) capable of simulating the full kinematics of the decay products. We subsequently used this code to produce differential predictions for the $H \to b\bar{b}$ decay in the Higgs boson rest frame, using the Durham jet algorithm. We found that the impact of the EFT-initiated pieces is very sensitive to the specific nature of the final-state phase-space selection criteria. Since the 2-body phase-space is suppressed relative to the 3-body one (at $\mathcal{O}(\alpha_s^2)$ where a clear distinction between the two can be made), requiring exactly two jets suppresses the impact of the EFT pieces. Further suppression occurs when two b-tagged jets are demanded, which can be also be traced back to the 3-body topology, since this matrix element is largest when the $g \to b\bar{b}$ splitting is quasi-collinear and the typical contribution is a single b-jet (containing the b and $\bar{b}$ pair) and a gluon jet. These effects are even more pronounced for the final-state charm quark, where due to the fact that $y_c < y_b$ the EFT^2 pieces are relatively enhanced with respect to the LO. Due to quasi-collinear logarithms, the mixed EFT terms are also more important for the $H \to c\bar{c}$ channel.

The EFT-initiated pieces spoil the relationship $\Gamma_{H \to q\bar{q}} \propto y_q^2$ and thus could pollute an extraction of the Higgs-quark coupling at colliders. Our results can be used to quantify the (QCD) impact of non-y_q^2 pieces, and their role in collider observables. The effects are maximally around a few percent (bottom) or 10-15% (charm), but can be significantly

suppressed by the selection criteria. Therefore, any analysis at the HL-LHC, or especially future lepton colliders, should endeavor to model these pieces given the fiducial specifics of the analysis. Finally we note that a full phenomenological study at the LHC and FC of $H \to q\bar{q}$ including the full $\mathcal{O}(\alpha_s^3)$ prediction and EW corrections (which also induce a y_t dependence) is extremely motivated. We leave this analysis to a future study.

Acknowledgments

A Renormalization coefficients

In this appendix we provide a list of the renormalization coefficients needed in our calculation. The gluon wavefunction renormalization coefficient is given by

$$Z_A^{\text{OS}} = 1 - \frac{\alpha_s}{4\pi} \frac{4T_R}{3\epsilon} \Gamma(1+\epsilon) \sum_{i \in n_h} \left(\frac{\mu^2}{m_i^2} \right)^{\epsilon} + \mathcal{O}\left(\alpha_s^2 \right) , \tag{A.1}$$

and for the strong coupling α_s,

$$Z_{\alpha_s}^{\overline{\text{MS}}} = 1 - \frac{\alpha_s}{4\pi} \frac{1}{\epsilon} \left(\frac{11}{3} C_A - \frac{8}{3} T_R\, n_f \right) + \mathcal{O}(\alpha_s^2) , \tag{A.2}$$

where n_f is the combined number of light flavors and heavy flavors ($n_f = 5$ in our calculations). For the heavy quark wavefunction,

$$Z_Q^{\text{OS}} = 1 - \frac{\alpha_s}{4\pi} C_f\, \Gamma(1+\epsilon) \left(\frac{\mu^2}{m_Q^2} \right)^{\epsilon} \frac{(3-2\epsilon)}{\epsilon\,(1-2\epsilon)} + \mathcal{O}(\alpha_s^2) \tag{A.3}$$

and heavy quark masses,

$$Z_{m_Q}^{\text{OS}} = -\frac{\alpha_s}{4\pi} C_f\, \Gamma(1+\epsilon) \left(\frac{\mu^2}{m_Q^2} \right)^{\epsilon} \frac{(3-2\epsilon)}{\epsilon\,(1-2\epsilon)} + \mathcal{O}(\alpha_s^2) . \tag{A.4}$$

Finally, the Yukawa couplings are renormalized using

$$Z_{y_b}^{\overline{\text{MS}}} = 1 + \frac{\alpha_s}{4\pi} \left(-\frac{3C_f}{\epsilon} \right) + \left(\frac{\alpha_s}{4\pi} \right)^2 \left[C_f^2 \left(\frac{9}{2\epsilon^2} - \frac{3}{4\epsilon} \right) \right. \tag{A.5}$$

$$\left. + C_f\, C_A \left(\frac{11}{2\epsilon^2} - \frac{97}{12\epsilon} \right) + C_f n_f \left(-\frac{1}{\epsilon^2} + \frac{5}{6\epsilon} \right) \right] + \mathcal{O}(\alpha_s^3) .$$

In order to renormalize the Wilson coefficient C_2, the heavy-quark mass renormalization is also needed in the $\overline{\text{MS}}$ scheme,

$$Z_m^{\overline{\text{MS}}} = 1 + \frac{\alpha_s}{4\pi} \left(-\frac{3C_f}{\epsilon} \right) + \left(\frac{\alpha_s}{4\pi} \right)^2 \left[C_f^2 \left(\frac{9}{2\epsilon^2} - \frac{3}{4\epsilon} \right) \right. \tag{A.6}$$

$$\left. + C_f\, C_A \left(\frac{11}{2\epsilon^2} - \frac{97}{12\epsilon} \right) + C_f n_f \left(-\frac{1}{\epsilon^2} + \frac{5}{6\epsilon} \right) \right] + \mathcal{O}(\alpha_s^3) .$$

Eqs. (2.20)–(2.21) define the matching coefficients C_1 and C_2 in terms of $\Delta_H^{(i)}$ and $\Delta_F^{(i)}$. In this calculation for C_1 we need the following [36],

$$\Delta_H^{(1)} = \left(\frac{11}{4} - \frac{1}{6} \log \frac{\mu^2}{m_t^2} \right) , \tag{A.7}$$

and for C_2,

$$\Delta_F^{(2)} = \left(\frac{5}{18} - \frac{1}{3} \log \frac{\mu^2}{m_t^2} \right) \tag{A.8}$$

$$\Delta_F^{(3)} = \frac{311}{1296} + \frac{5}{3}\zeta(3) - \frac{175}{108} \log \frac{\mu^2}{m_t^2} - \frac{29}{36} \log^2 \frac{\mu^2}{m_t^2} + n_l \left(\frac{53}{216} + \frac{1}{18} \log^2 \frac{\mu^2}{m_t^2} \right) , \tag{A.9}$$

where we note that these results are defined in the $\overline{\text{MS}}$ scheme with $N_c = 3$.

B Definition of canonical master integrals

In this appendix we provide the exact definitions of the master integrals satisfying the canonical differential equation (2.44):

$$I_1 = \epsilon^2 \, \mathcal{T}_1 \, , \qquad\qquad\qquad I_2 = \epsilon^2 \, \mathcal{T}_2 \, ,$$

$$I_3 = \epsilon^2 \, m_b^2 \, m_c^2 \, \mathcal{T}_3 \, , \qquad I_4 = \epsilon^2 \, m_b^3 \, m_c \, \frac{\left(m_H^2 - \lambda_{m_b}\right) \Lambda_{m_c}}{\left(m_H^2 - \lambda_{m_c}\right) \Lambda_{m_b}} \left(2\mathcal{T}_3 + \mathcal{T}_4\right) \, ,$$

$$I_5 = -\epsilon^2 \, m_b^2 \, m_H^2 \, \mathcal{T}_5 \, , \qquad I_6 = -\epsilon^2 \, m_b^2 \, m_H^2 \, \mathcal{T}_6 \, ,$$

$$I_7 = -\epsilon^2 \, m_b^2 \, \lambda_{m_b} \left[\left(\frac{1}{2} + \frac{m_H^2}{\lambda_{m_b}} \right) \mathcal{T}_6 + \mathcal{T}_7 \right] \, , \qquad I_8 = -\epsilon^2 \, m_b^2 \, \lambda_{m_b} \, \mathcal{T}_8 \, ,$$

$$I_9 = -\epsilon^2 \, m_b^2 \, \lambda_{m_b} \, \mathcal{T}_9 \, , \qquad\qquad I_{10} = \epsilon^3 \, m_b^2 \, m_H^2 \, \frac{m_H^2 - 4m_c^2 - \lambda_{m_c}}{m_H^2 - \lambda_{m_c}} \, \mathcal{T}_{10} \, ,$$

$$I_{11} = \epsilon^3 \, m_b^2 \, m_H^2 \, \frac{m_H^2 - 4m_c^2 - \lambda_{m_c}}{m_H^2 - \lambda_{m_c}} \, \mathcal{T}_{11} \, ,$$

$$I_{12} = -\epsilon^2 \frac{m_b^2 \, \lambda_{m_b}}{4 m_H^2} \left[\left(m_H^2 + \lambda_{m_c}\right) \left(\mathcal{T}_6 + 2\,\mathcal{T}_7\right) + 4\, m_b^2 \, m_c^2 \, \lambda_{m_c} \, \mathcal{T}_{12} \right]$$

$$I_{13} = \epsilon^3 \, m_b^2 \, m_H^2 \, \frac{m_H^2 - 4m_c^2 - \lambda_{m_c}}{m_H^2 - \lambda_{m_c}} \, \mathcal{T}_{13} \, , \qquad I_{14} = \epsilon^3 \, m_b^2 \, m_H^2 \, \frac{m_H^2 - 4m_c^2 - \lambda_{m_c}}{m_H^2 - \lambda_{m_c}} \, \mathcal{T}_{14} \, ,$$

$$I_{15} = -\epsilon^2 \frac{m_b^2 \, \lambda_{m_b} \left(m_H^2 + \lambda_{m_c}\right)}{4 \, m_H^2} \left[\mathcal{T}_6 + 2\,\mathcal{T}_7 - 4 \frac{m_b^2 \, m_c^2 \left(m_H^4 - \lambda_{m_b} \lambda_{m_c}\right)}{\lambda_{m_b}} \mathcal{T}_{12} \right.$$

$$\left. -4\epsilon \frac{m_H^2}{\lambda_{m_b}} \left(2\,\mathcal{T}_{13} + \mathcal{T}_{14}\right) \right] - \epsilon^2 (1 + 2\epsilon) \, m_b^4 \, m_c^2 \, m_H^2 \, \mathcal{T}_{15} \, ,$$

$$I_{16} = \epsilon^3 \, m_b^4 \, \lambda_{m_b} \, \lambda_{m_c} \, \mathcal{T}_{16} \, , \qquad\qquad I_{17} = \epsilon^2 \, m_b^4 \, m_H^2 \lambda_{m_b} \, \mathcal{T}_{17} \, ,$$

$$I_{18} = \epsilon^3 \, m_b^4 \, \lambda_{m_b} \, \lambda_{m_c} \, \mathcal{T}_{18} \, , \qquad\qquad I_{19} = -\epsilon^3 \, (1 - 2\epsilon) \, m_b^2 \, m_H^2 \, \mathcal{T}_{19} \, ,$$

$$I_{20} = -\epsilon^4 \frac{m_b^4 \, m_H^4 \left(m_H^2 - 4m_c^2 - \lambda_{m_c}\right)}{m_H^2 - \lambda_{m_c}} \, \mathcal{T}_{20} \, , \tag{B.1}$$
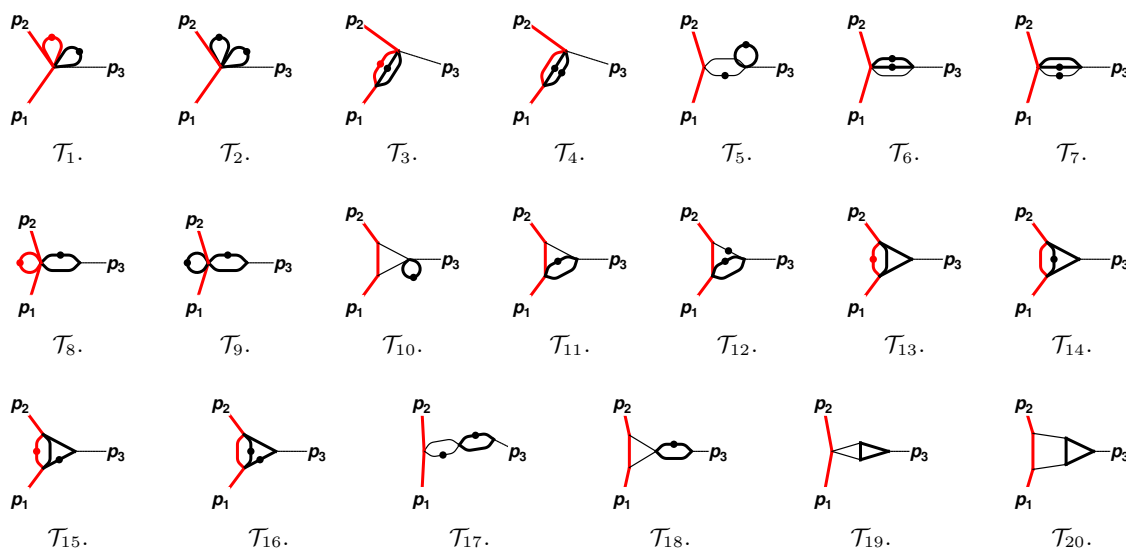
Figure 9. Master integrals $\mathcal{T}_{1...20}$ for the leading-order bottom Yukawa contributions to the Higgs boson decay into charm quarks. Thin black lines represent massless propagators, while thick black lines and red lines represent massive propagators with mass m_b or m_c respectively. Dots represent additional powers of the propagator.

where we defined the abbreviations $\lambda_m = \sqrt{m_H^2}\sqrt{m_H^2 - 4\,m^2}$ and $\Lambda_m = \sqrt{m_H^2 - 2\,m^2 - \lambda_m}$. The integrals $\mathcal{T}_i$ appearing above are depicted in figure 9. The definitions and expressions of the canonical master integrals are also given in the supplementary material and also accompanying the `arXiv` submission of this publication.

References

[1] ATLAS collaboration, *Observation of a new particle in the search for the Standard Model Higgs boson with the ATLAS detector at the LHC*, *Phys. Lett. B* **716** (2012) 1 [`arXiv:1207.7214`] [INSPIRE].

[2] CMS collaboration, *Observation of a new boson at a mass of* 125 *GeV with the CMS experiment at the LHC*, *Phys. Lett. B* **716** (2012) 30 [`arXiv:1207.7235`] [INSPIRE].

[3] CMS collaboration, *Precise determination of the mass of the Higgs boson and tests of compatibility of its couplings with the Standard Model predictions using proton collisions at 7 and 8 TeV*, *Eur. Phys. J. C* **75** (2015) 212 [`arXiv:1412.8662`] [INSPIRE].

[4] CMS collaboration, *Measurements of properties of the Higgs boson decaying into the four-lepton final state in pp collisions at* $\sqrt{s} = 13$ *TeV*, *JHEP* **11** (2017) 047 [`arXiv:1706.09936`] [INSPIRE].

[5] ATLAS and CMS collaborations, *Combined measurement of the Higgs boson mass in pp collisions at $\sqrt{s} = 7$ and 8 TeV with the ATLAS and CMS experiments*, *Phys. Rev. Lett.* **114** (2015) 191803 [arXiv:1503.07589] [INSPIRE].

[6] ATLAS collaboration, *Measurements of the Higgs boson production and decay rates and coupling strengths using pp collision data at $\sqrt{s} = 7$ and 8 TeV in the ATLAS experiment*, *Eur. Phys. J. C* **76** (2016) 6 [arXiv:1507.04548] [INSPIRE].

[7] M. Cepeda et al., *Report from working group 2: Higgs physics at the HL-LHC and HE-LHC*, *CERN Yellow Rep. Monogr.* **7** (2019) 221 [arXiv:1902.00134] [INSPIRE].

[8] TLEP DESIGN STUDY WORKING GROUP collaboration, *First look at the physics case of TLEP*, *JHEP* **01** (2014) 164 [arXiv:1308.6176] [INSPIRE].

[9] H. Baer et al., eds., *The International Linear Collider technical design report — volume 2: physics*, arXiv:1306.6352 [INSPIRE].

[10] FCC collaboration, *FCC-ee: the lepton collider. Future Circular Collider conceptual design report volume 2*, *Eur. Phys. J. ST* **228** (2019) 261 [INSPIRE].

[11] ATLAS collaboration, *Search for the decay of the Higgs boson to charm quarks with the ATLAS experiment*, *Phys. Rev. Lett.* **120** (2018) 211802 [arXiv:1802.04329] [INSPIRE].

[12] CMS collaboration, *A search for the Standard Model Higgs boson decaying to charm quarks*, *JHEP* **03** (2020) 131 [arXiv:1912.01662] [INSPIRE].

[13] E. Braaten and J.P. Leveille, *Higgs boson decay and the running mass*, *Phys. Rev. D* **22** (1980) 715 [INSPIRE].

[14] S.G. Gorishnii, A.L. Kataev and S.A. Larin, *The width of Higgs boson decay into hadrons: three loop corrections of strong interactions*, *Sov. J. Nucl. Phys.* **40** (1984) 329 [*Yad. Fiz.* **40** (1984) 517] [INSPIRE].

[15] S.G. Gorishnii, A.L. Kataev, S.A. Larin and L.R. Surguladze, *Corrected three loop QCD correction to the correlator of the quark scalar currents and $\gamma_{\rm tot}(H^0 \to {\rm hadrons})$*, *Mod. Phys. Lett. A* **5** (1990) 2703 [INSPIRE].

[16] S.G. Gorishnii, A.L. Kataev, S.A. Larin and L.R. Surguladze, *Scheme dependence of the next to next-to-leading QCD corrections to $\Gamma_{\rm tot}(H^0 \to {\rm hadrons})$ and the spurious QCD infrared fixed point*, *Phys. Rev. D* **43** (1991) 1633 [INSPIRE].

[17] A.L. Kataev and V.T. Kim, *The effects of the QCD corrections to $\Gamma(H^0 \to b\bar{b})$*, *Mod. Phys. Lett. A* **9** (1994) 1309 [INSPIRE].

[18] L.R. Surguladze, *Quark mass effects in fermionic decays of the Higgs boson in $O(\alpha_s^2)$ perturbative QCD*, *Phys. Lett. B* **341** (1994) 60 [hep-ph/9405325] [INSPIRE].

[19] S.A. Larin, T. van Ritbergen and J.A.M. Vermaseren, *The large top quark mass expansion for Higgs boson decays into bottom quarks and into gluons*, *Phys. Lett. B* **362** (1995) 134 [hep-ph/9506465] [INSPIRE].

[20] K.G. Chetyrkin and A. Kwiatkowski, *Second order QCD corrections to scalar and pseudoscalar Higgs decays into massive bottom quarks*, *Nucl. Phys. B* **461** (1996) 3 [hep-ph/9505358] [INSPIRE].

[21] K.G. Chetyrkin, *Correlator of the quark scalar currents and $\Gamma_{\rm tot}(H \to {\rm hadrons})$ at $O(\alpha_s^3)$ in pQCD*, *Phys. Lett. B* **390** (1997) 309 [hep-ph/9608318] [INSPIRE].

[22] P.A. Baikov, K.G. Chetyrkin and J.H. Kühn, *Scalar correlator at $O(\alpha_s^4)$, Higgs decay into b-quarks and bounds on the light quark masses*, *Phys. Rev. Lett.* **96** (2006) 012003 [hep-ph/0511063] [INSPIRE].

[23] A. Dabelstein and W. Hollik, *Electroweak corrections to the fermionic decay width of the standard Higgs boson*, *Z. Phys. C* **53** (1992) 507 [INSPIRE].

[24] L. Mihaila, B. Schmidt and M. Steinhauser, *$\Gamma(H \to b\bar{b})$ to order $\alpha\alpha_s$*, *Phys. Lett. B* **751** (2015) 442 [arXiv:1509.02294] [INSPIRE].

[25] E. Chaubey and S. Weinzierl, *Two-loop master integrals for the mixed QCD-electroweak corrections for $H \to b\bar{b}$ through a $Ht\bar{t}$-coupling*, *JHEP* **05** (2019) 185 [arXiv:1904.00382] [INSPIRE].

[26] C. Anastasiou, F. Herzog and A. Lazopoulos, *The fully differential decay rate of a Higgs boson to bottom-quarks at NNLO in QCD*, *JHEP* **03** (2012) 035 [arXiv:1110.2368] [INSPIRE].

[27] V. Del Duca, C. Duhr, G. Somogyi, F. Tramontano and Z. Trócsányi, *Higgs boson decay into b-quarks at NNLO accuracy*, *JHEP* **04** (2015) 036 [arXiv:1501.07226] [INSPIRE].

[28] W. Bernreuther, L. Chen and Z.-G. Si, *Differential decay rates of CP-even and CP-odd Higgs bosons to top and bottom quarks at NNLO QCD*, *JHEP* **07** (2018) 159 [arXiv:1805.06658] [INSPIRE].

[29] A. Behring and W. Bizoń, *Higgs decay into massive b-quarks at NNLO QCD in the nested soft-collinear subtraction scheme*, *JHEP* **01** (2020) 189 [arXiv:1911.11524] [INSPIRE].

[30] R. Mondini, M. Schiavi and C. Williams, *N^3LO predictions for the decay of the Higgs boson to bottom quarks*, *JHEP* **06** (2019) 079 [arXiv:1904.08960] [INSPIRE].

[31] R. Mondini and C. Williams, *$H \to b\bar{b}j$ at next-to-next-to-leading order accuracy*, *JHEP* **06** (2019) 120 [arXiv:1904.08961] [INSPIRE].

[32] T. Ahmed, M. Mahakhud, P. Mathews, N. Rana and V. Ravindran, *Two-loop QCD corrections to $Higgs \to b + \bar{b} + g$ amplitude*, *JHEP* **08** (2014) 075 [arXiv:1405.2324] [INSPIRE].

[33] A. Primo, G. Sasso, G. Somogyi and F. Tramontano, *Exact top Yukawa corrections to Higgs boson decay into bottom quarks*, *Phys. Rev. D* **99** (2019) 054013 [arXiv:1812.07811] [INSPIRE].

[34] W. Bernreuther et al., *Two-loop QCD corrections to the heavy quark form-factors: the vector contributions*, *Nucl. Phys. B* **706** (2005) 245 [hep-ph/0406046] [INSPIRE].

[35] K. Melnikov and T.v. Ritbergen, *The three loop relation between the MS-bar and the pole quark masses*, *Phys. Lett. B* **482** (2000) 99 [hep-ph/9912391] [INSPIRE].

[36] K.G. Chetyrkin, B.A. Kniehl and M. Steinhauser, *Decoupling relations to $O(\alpha_s^3)$ and their connection to low-energy theorems*, *Nucl. Phys. B* **510** (1998) 61 [hep-ph/9708255] [INSPIRE].

[37] C. Anastasiou, N. Deutschmann and A. Schweitzer, *Quark mass effects in two-loop Higgs amplitudes*, *JHEP* **07** (2020) 113 [arXiv:2001.06295] [INSPIRE].

[38] M. Cacciari, F.A. Dreyer, A. Karlberg, G.P. Salam and G. Zanderighi, *Fully differential vector-boson-fusion Higgs production at next-to-next-to-leading order*, *Phys. Rev. Lett.* **115** (2015) 082002 [*Erratum ibid.* **120** (2018) 139901] [arXiv:1506.02660] [INSPIRE].

[39] J. Gaunt, M. Stahlhofen, F.J. Tackmann and J.R. Walsh, *N-jettiness subtractions for NNLO QCD calculations*, *JHEP* **09** (2015) 058 [arXiv:1505.04794] [INSPIRE].

[40] R. Boughezal, C. Focke, X. Liu and F. Petriello, *W-boson production in association with a jet at next-to-next-to-leading order in perturbative QCD*, *Phys. Rev. Lett.* **115** (2015) 062002 [arXiv:1504.02131] [INSPIRE].

[41] S. Catani and M.H. Seymour, *A general algorithm for calculating jet cross-sections in NLO QCD*, *Nucl. Phys. B* **485** (1997) 291 [*Erratum ibid.* **510** (1998) 503] [hep-ph/9605323] [INSPIRE].

[42] S. Catani, S. Dittmaier, M.H. Seymour and Z. Trócsányi, *The dipole formalism for next-to-leading order QCD calculations with massive partons*, *Nucl. Phys. B* **627** (2002) 189 [hep-ph/0201036] [INSPIRE].

[43] S. Dittmaier, *A general approach to photon radiation off fermions*, *Nucl. Phys. B* **565** (2000) 69 [hep-ph/9904440] [INSPIRE].

[44] P. Nogueira, *Automatic Feynman graph generation*, *J. Comput. Phys.* **105** (1993) 279 [INSPIRE].

[45] M. Jamin and M.E. Lautenbacher, *TRACER: version* 1.1. *A Mathematica package for gamma algebra in arbitrary dimensions*, *Comput. Phys. Commun.* **74** (1993) 265 [INSPIRE].

[46] R.N. Lee, *Presenting LiteRed: a tool for the Loop InTEgrals REDuction*, arXiv:1212.2685 [INSPIRE].

[47] R.N. Lee, *LiteRed* 1.4*: a powerful tool for reduction of multiloop integrals*, *J. Phys. Conf. Ser.* **523** (2014) 012059 [arXiv:1310.1145] [INSPIRE].

[48] A. von Manteuffel and C. Studerus, *Reduze* 2 — *distributed Feynman integral reduction*, arXiv:1201.4330 [INSPIRE].

[49] P. Mastrolia, M. Passera, A. Primo and U. Schubert, *Master integrals for the NNLO virtual corrections to µe scattering in QED: the planar graphs*, *JHEP* **11** (2017) 198 [arXiv:1709.07435] [INSPIRE].

[50] S. Di Vita, T. Gehrmann, S. Laporta, P. Mastrolia, A. Primo and U. Schubert, *Master integrals for the NNLO virtual corrections to qq̄ → tt̄ scattering in QCD: the non-planar graphs*, *JHEP* **06** (2019) 117 [arXiv:1904.10964] [INSPIRE].

[51] R. Ellis and G. Zanderighi, *Scalar one-loop integrals for QCD*, *JHEP* **02** (2008) 002 [arXiv:0712.1851] [INSPIRE].

[52] S. Carrazza, R.K. Ellis and G. Zanderighi, *QCDLoop: a comprehensive framework for one-loop scalar integrals*, *Comput. Phys. Commun.* **209** (2016) 134 [arXiv:1605.03181] [INSPIRE].

[53] J. Fleischer, A.V. Kotikov and O.L. Veretin, *Analytic two loop results for selfenergy type and vertex type diagrams with one nonzero mass*, *Nucl. Phys. B* **547** (1999) 343 [hep-ph/9808242] [INSPIRE].

[54] A.I. Davydychev and M. Kalmykov, *Massive Feynman diagrams and inverse binomial sums*, *Nucl. Phys. B* **699** (2004) 3 [hep-th/0303162] [INSPIRE].

[55] A.V. Kotikov, *Differential equations method: new technique for massive Feynman diagrams calculation*, *Phys. Lett. B* **254** (1991) 158 [INSPIRE].

[56] J. Fleischer, A.V. Kotikov and O.L. Veretin, *The differential equation method: calculation of vertex type diagrams with one nonzero mass*, *Phys. Lett. B* **417** (1998) 163 [hep-ph/9707492] [INSPIRE].

[57] E. Remiddi, *Differential equations for Feynman graph amplitudes*, *Nuovo Cim. A* **110** (1997) 1435 [hep-th/9711188] [INSPIRE].

[58] T. Gehrmann and E. Remiddi, *Differential equations for two loop four point functions*, *Nucl. Phys. B* **580** (2000) 485 [hep-ph/9912329] [INSPIRE].

[59] M. Argeri et al., *Magnus and Dyson series for master integrals*, *JHEP* **03** (2014) 082 [arXiv:1401.2979] [INSPIRE].

[60] S. Di Vita, P. Mastrolia, U. Schubert and V. Yundin, *Three-loop master integrals for ladder-box diagrams with one massive leg*, *JHEP* **09** (2014) 148 [arXiv:1408.3107] [INSPIRE].

[61] A.B. Goncharov, *Polylogarithms in arithmetic and geometry*, in *Proceedings of the International Congress of Mathematicians*, Birkhäuser, Basel, Switzerland (1995), pg. 374.

[62] E. Remiddi and J.A.M. Vermaseren, *Harmonic polylogarithms*, *Int. J. Mod. Phys. A* **15** (2000) 725 [hep-ph/9905237] [INSPIRE].

[63] T. Gehrmann and E. Remiddi, *Numerical evaluation of two-dimensional harmonic polylogarithms*, *Comput. Phys. Commun.* **144** (2002) 200 [hep-ph/0111255] [INSPIRE].

[64] J. Vollinga and S. Weinzierl, *Numerical evaluation of multiple polylogarithms*, *Comput. Phys. Commun.* **167** (2005) 177 [hep-ph/0410259] [INSPIRE].

[65] S. Borowka, J. Carter and G. Heinrich, *Numerical evaluation of multi-loop integrals for arbitrary kinematics with SecDec 2.0*, *Comput. Phys. Commun.* **184** (2013) 396 [arXiv:1204.4152] [INSPIRE].

[66] S. Borowka, G. Heinrich, S.P. Jones, M. Kerner, J. Schlenk and T. Zirke, *SecDec-3.0: numerical evaluation of multi-scale integrals beyond one loop*, *Comput. Phys. Commun.* **196** (2015) 470 [arXiv:1502.06595] [INSPIRE].

[67] J.M. Campbell and R. Ellis, *An update on vector boson pair production at hadron colliders*, *Phys. Rev. D* **60** (1999) 113006 [hep-ph/9905386] [INSPIRE].

[68] J.M. Campbell, R. Ellis and C. Williams, *Vector boson pair production at the LHC*, *JHEP* **07** (2011) 018 [arXiv:1105.0020] [INSPIRE].

[69] J.M. Campbell, R.K. Ellis and W.T. Giele, *A multi-threaded version of MCFM*, *Eur. Phys. J. C* **75** (2015) 246 [arXiv:1503.06182] [INSPIRE].

[70] N. Brown and W. Stirling, *Jet cross-sections at leading double logarithm in e^+e^- annihilation*, *Phys. Lett. B* **252** (1990) 657 [INSPIRE].

[71] S. Catani, Y.L. Dokshitzer, M. Olsson, G. Turnock and B.R. Webber, *New clustering algorithm for multi-jet cross-sections in e^+e^- annihilation*, *Phys. Lett. B* **269** (1991) 432 [INSPIRE].